Mon. Not. R. Astron. Soc. **000**, 000–000 (2002)

A Comparison of Gas Dynamics in SPH and Semi-analytic Models of Galaxy Formation

John C. Helly[1], Shaun Cole[1], Carlos S. Frenk[1], Carlton M. Baugh[1], Andrew Benson[2], Cedric Lacey[1], Frazer R. Pearce[3]

[1] *Department of Physics, University of Durham, Science Laboratories, South Road, Durham DH1 3LE, United Kingdom*
[2] *California Institute of Technology, MC105-24, Pasadena CA 91125, USA*
[3] *Physics and Astronomy, University of Nottingham, Nottingham, NG7 2RD*

27 February 2002

ABSTRACT

We compare the results of two techniques used to calculate the evolution of cooling gas during galaxy formation: Smooth Particle Hydrodynamics (SPH) simulations and semi-analytic modelling. We improve upon the earlier statistical approach of Benson et al. by comparing the evolution of galaxies on an object-by-object basis in the two treatments. First, we describe a new, mass-conserving method for extracting merger trees of dark matter halos from N-body simulations. We show that, when the resolution of the simulation is properly taken into account, the semi-analytic model of Cole et al gives similar results whether N-body or Monte-Carlo merger trees are used. We then generate a "stripped-down" version of the Cole et al model which includes only shock heating and radiative cooling of gas and which is adjusted to mimic the resolution and other parameters of a comparison SPH simulation as closely as possible. We compare the total mass of gas that cools in halos of different mass as a function of redshift as well as the masses and spatial distribution of individual "galaxies." At redshift $z = 0$, the cooled gas mass in well-resolved halos agrees remarkably well (to better than $\sim$20%) in the SPH simulation and stripped-down semi-analytic model. At high redshift, resolution effects in the simulation become increasingly important and, as a result, more gas tends to cool in low mass halos in the SPH simulation than in the semi-analytic model. The cold gas mass function of individual galaxies in the two treatments at $z = 0$ also agrees very well and, when the effects of mergers are accounted for, the masses of individual galaxies and their 2-point correlation functions are also in excellent agreement in the two treatments. Thus, our comparison confirms and extends the earlier conclusion of Benson et al. that SPH simulations and semi-analytic models give consistent results for the evolution of cooling galactic gas.

Key words: galaxies: formation

1 INTRODUCTION

Hierarchical models of galaxy formation must describe both the growth and collapse of density perturbations to form dark matter halos and the baryonic processes which lead to the formation of stars. Despite uncertainty as to the exact nature of the dark matter itself, the formation and evolution of dark matter halos appears to be reasonably well understood. The two main approaches to this problem are direct numerical simulations and analytic techniques such as the Press-Schechter theory (Press & Schechter 1974) and its extensions (Bond et al. 1991; Bower 1991; Lacey & Cole 1993). Encouragingly, the mass functions of dark matter halos predicted using these very different approaches are found to agree to within 50% (Gross et al. 1998; Governato et al. 1999). Unfortunately, the behaviour of the baryonic component of the universe is more complex and less well understood. While the dynamics of the dark matter are determined by gravitational forces alone, gas is subject to hydrodynamical forces and radiative effects.

The two most commonly used approaches to the problem of galaxy formation are semi-analytic models and numerical simulations. Both techniques attempt to follow the development of galaxies from primordial density fluctuations. In semi-analytic models, merger histories for dark matter halos may be taken directly from dark matter simulations (e.g. Kauffmann et al. 1999; van Kampen et al. 1999) or

generated using Monte-Carlo algorithms based on analytical theories of the evolution of cosmological density perturbations, such as extended Press Schechter theory (e.g. Kauffmann & White 1993; Cole et al. 2000). Simple analytic modelling is used to follow the evolution of the baryonic component, including prescriptions for processes such as star formation and its possible effects on the remaining gas. Semi-analytic models (e.g. Cole 1991;Cole et al. 1994,2000;White & Frenk 1991; Lacey & Silk 1991; Somerville & Primack 1999) have successfully reproduced many observable properties of galaxies, such as the local field galaxy luminosity function and distributions of colour and morphology. When combined with N-body simulations, semi-analytic models have also successfully reproduced galaxy clustering properties (e.g. Kauffmann et al. 1999; Benson et al. 2000; Wechsler et al. 2001).

While Eulerian numerical techniques may be employed in the modelling of galaxy formation in cosmological volumes (e.g. Cen & Ostriker 2000), here we concentrate on the Lagrangian method known as smoothed particle hydrodynamics, first described by Lucy (1977) and Gingold & Monaghan (1977). SPH simulations have been able to predict the formation of objects of approximately galactic mass with appropriate abundances in a cosmological context (e.g. Katz, Hernquist & Weinberg 1992; Navarro & White 1993; Evrard, Summers & Davis 1994; Steinmetz & Müller 1995; Katz, Weinberg & Hernquist 1996; Frenk et al. 1996; Navarro & Steinmetz 1999; Pearce et al. 1999) and allow the investigation of the dynamics of galaxies within clusters and the spatial distribution of galaxies.

Semi-analytic and SPH galaxy formation models rely on very different sets of assumptions. For example, semi-analytic models assume that dark matter halos are spherically symmetric and that infalling gas is shock-heated to the virial temperature of the halo, whereas SPH simulations impose no restrictions on halo geometry but assume that continuous distributions of gas and dark matter may be well represented by a limited number of discrete particles. Consequently, SPH and semi-analytic models have complementary strengths and weaknesses. Semi-analytic models are computationally much cheaper than simulations, which allows extremely high mass resolution in halo merger trees and more thorough investigation of the effects of varying parameters or the treatment of particular processes. SPH simulations contain fewer simplifying assumptions but have limited dynamic range and without sufficiently large numbers of particles may suffer from numerical effects.

The aim of this paper is to compare SPH and semi-analytic treatments of the gas dynamics involved in galaxy formation in order to gauge the effects of the uncertainties present in the two techniques. A previous comparison carried out by Benson et al. (2001a) found that SPH and semi-analytic models give similar results for the thermodynamic evolution of cooling gas in cosmological volumes. In particular, the global fractions of hot gas, cold dense gas and uncollapsed gas agreed to within 25% and the mass of gas in galaxies in the most massive halos differed by no more than 50%. However, their analysis was restricted to a statistical comparison because their semi-analytic model employed merger histories created using a Monte-Carlo algorithm, that of Cole et al. (2000). We improve on the work of Benson et al. by calculating the merger trees directly from the simulations so that the merger histories of the halos in the semi-analytic and SPH treatments are the same. This removes a source of uncertainty from the comparison, since any differences between the models must be due to differences in the treatment of the *baryonic* component. Our method also allows a comparison between halos on an individual basis and lets us investigate whether the dependence of the mass of gas which cools in a halo on the halo's merger history is the same in the SPH and semi-analytic cases.

Our approach is that of "modelling a model", using a semi-analytic model to reproduce the behaviour of the simulation including the effects of limited mass resolution. Since we are interested primarily in the rate at which cooling occurs in the two models we use a simulation which allows radiative cooling but which does not include any prescription for star formation or feedback. We attempt to model this simulation using a "stripped down" semi-analytic model which also neglects these phenomena. Hierarchical models of galaxy formation without feedback predict that most of the gas in the universe cools in low mass objects at high redshift (e.g. White & Rees 1978; Cole 1991; White & Frenk 1991). Consequently, we cannot expect either our SPH simulation or our stripped down semi-analytic model to cool realistic quantities of gas, and where differences between the two approaches are found it may not be possible to conclude that one is more "correct" than the other. However, the changes which must be made to the semi-analytic model may provide insight into the level of agreement between the two techniques and the reasons for any discrepancies.

This paper is laid out as follows. In Section 2 the techniques used to obtain the merger histories of simulated dark matter halos are explained. In Section 3 we incorporate these merger histories into the semi-analytic model of Cole et al. and in Section 4 we use this model to compare SPH and semi-analytic treatments of the gas dynamics of galaxy formation. Our conclusions are presented in Section 5.

2 EXTRACTING MERGER TREES

We first present the methods used to calculate the merger histories of dark matter halos identified in an N-body simulation. The first of the two simulations used here, which will be referred to as the GIF simulation, was run by the Virgo Consortium using a parallel adaptive particle-particle particle mesh ($\mathrm{AP^3M}$) code known as Hydra (Couchman, Thomas & Pearce 1995; Pearce & Couchman 1997) as part of the GIF project. The simulation adopts the ΛCDM cosmology with mean mass density parameter $\Omega_0 = 0.3$, cosmological constant $\Lambda_0 = 0.7$ in units of $3H_0^2/c^2$, power spectrum shape parameter $\Gamma = 0.21$, present day rms linear fluctuation amplitude in $8h^{-1}$Mpc spheres $\sigma_8 = 0.90$, and Hubble constant $h = 0.7$ in units of $100\mathrm{kms}^{-1}\mathrm{Mpc}^{-1}$. It contains 256^3 dark matter particles each of mass $1.4 \times 10^{10} h^{-1} M_\odot$ in a box of side $141.3h^{-1}$Mpc. The gravitational softening length in the simulation is $30h^{-1}$kpc at $z = 0$. This simulation is described in more detail by Jenkins et al. (1998), where it is referred to as ΛCDM2, and by Kauffmann et al. (1999).

In Section 3 we use the GIF simulation to compare galaxy formation models in which merger trees are either

constructed using the Monte Carlo method of Cole et al. (2000) or obtained directly from an N-body simulation.

2.1 Identifying Halos

In order to construct merger histories, or "merger trees", for dark matter halos in an N-body simulation, a catalogue of halos must be produced for each simulation output time using a group finding algorithm. The algorithm used here is the "friends of friends" (FOF) method of Davis et al. (1985), which simply links together any particles with separations less than the linking length b, usually expressed in terms of the mean separation. Given sufficiently large numbers of particles in each object, the FOF algorithm finds regions bounded by a surface of constant density. The density threshold is proportional to $1/b^3$.

The FOF approach has the advantage that it imposes no constraints on the geometry of the halos identified, but it may occasionally artificially join two nearby halos if a transient "bridge" of a few particles forms between them. It will be seen in Section 2.2 that this can cause problems when attempting to generate merger trees using FOF group catalogues, and a method of identifying and splitting artificially joined halos is described in Section 2.2.

The usual choice for the linking length in cosmologies with $\Omega = 1$ is $b = 0.2$ (e.g. Lacey & Cole 1994), which identifies halos with a mean density similar to that predicted by the top hat spherical collapse model (Cole & Lacey 1996). However, in cosmologies with $\Omega < 1$ there is no rigorous justification for any particular choice. Here, we choose to set $b = 0.2$ at all redshifts as in the $\Omega = 1$ case. See Jenkins et al. (2001) for further discussion.

The other parameter needed by the FOF algorithm is the minimum number of particles, $N_{\rm min}$, required to constitute a group. It is important that $N_{\rm min}$ be as small as possible, since detailed merger trees can only be obtained for halos much larger than the smallest resolvable group. Kauffmann et al. (1999) found that in their simulations groups as small as ten particles are dynamically stable systems and that for 95% of these groups, 80% of the particles remain in the same group at subsequent times.

We therefore identify halos using a linking length $b = 0.2$ at all redshifts, with a minimum group size of ten particles. The resulting catalogues may still contain groups which consist of unbound particles which happen to be close together at this particular time step. To remove these, we follow Benson et al. (2001b) and calculate the total energy of each group. Unbound groups are not immediately discarded however, because they may only be unbound due to the presence of a small number of fast moving particles. The binding energy of each particle is calculated, and the least bound particle removed from the group. This is repeated until the group becomes bound. If half of the particles are removed or the group is reduced to less than $N_{\rm min}$ particles we discard the group.

2.2 Constructing N-body Merger Trees

In an idealised picture of the process of hierarchical structure formation (e.g. Press-Schechter theory), dark matter halos may increase in mass by mergers, but cannot lose mass. Consequently, any halo identified in a simulation prior to the final output time should still exist at subsequent output times, although it may have become subsumed within a larger halo through a merger. In any case, the constituent particles of the original halo should still all be members of a single group. It should therefore be possible to identify each halo in the simulation as a progenitor of a single halo at the next output time.

In practice there are several ways in which a halo can lose particles. Halos may be disrupted by tidal forces caused by other nearby halos. The masses of simulated halos can also fluctuate because the FOF algorithm imposes a somewhat arbitrary boundary on the halo and outlying particles which are considered group members at one time step may lie just beyond the boundary at the next time step.

The technique we use to determine merger histories is intended to take into account this uncertainty in the definition of a halo and a possible loss of particles. First, we consider two adjacent output times from the simulation, t_1 and t_2, where $t_2 > t_1$. Each halo at time t_1 is labelled as a progenitor of whichever halo at time t_2 contains the largest fraction of its particles. This process is repeated for all pairs of adjacent output times. It is then straightforward to trace the merger history of each halo which exists at the final output time. Fig. 1 shows an example of a merger tree created in this way for a halo with a mass of about $9 \times 10^{12} h^{-1} M_{\odot}$, or around 700 particles.

In the semi-analytic model used here, galaxies are assumed to form at the centres of dark matter halos, so the centre of each halo in the merger tree must be defined. We choose to follow Kauffmann et al. (1999), who identified the most bound dark matter particle in the halo as the position of any galaxy formation. We define the binding energy of a particle as the sum of its kinetic energy and the gravitational potential energy due to the other particles in the halo. This approach differs from that of Benson et al. , who associated the central galaxy in a halo with the centre of mass, since we require that the particle associated with the galaxy must remain in the halo at subsequent times. Once a galaxy forms it will be assumed to follow this particle until the parent halo merges with another halo and dynamical friction causes the galaxy to merge with the central galaxy of the new halo. We therefore check that the most bound particle of a halo remains a member of the same halo as the majority of the halo's constituent particles at the next output time. If this is not so, we choose the most bound particle from those which *are* in the correct halo at the later output time. This generally only occurs in smaller halos which may be easily disrupted.

During the construction of the merger trees, we also attempt to deal with the problem mentioned in Section 2.1 — the possibility that nearby halos may be artificially linked by the FOF algorithm. The problem occurs if two halos become temporarily linked by a transient "bridge" of particles which causes the FOF group finder to consider them as a single, large group. When the bridge is later broken, the group splits, leaving the two original halos. Our tree building method would identify the large, joined group as a progenitor of the larger of the two final groups.

These situations are identified by looking for groups at the earlier time t_1 whose particles are shared between two or more groups at the subsequent output time t_2. This indicates

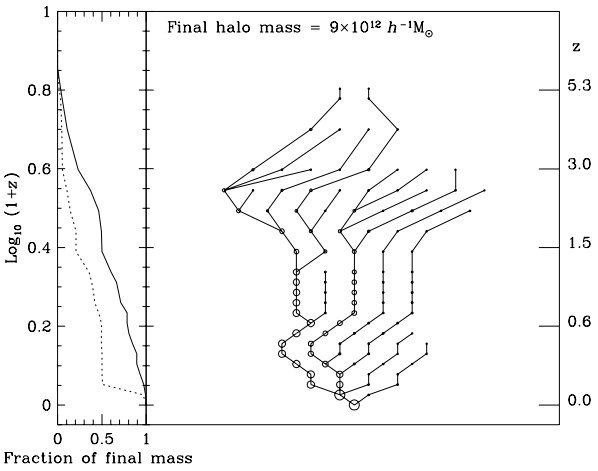

Figure 1. An example of a merger tree obtained from the GIF simulation for a halo of mass $9 \times 10^{12} h^{-1}\mathrm{M}_{\odot}$ at redshift $z = 0$. Each circle represents a dark matter halo identified in the simulation, the area of the circle being proportional to the halo mass. The solid line in the panel on the left-hand side shows the fraction of the final mass contained in progenitors as a function of redshift. The dotted line shows the fraction of the final mass contained in the largest progenitor as a function of redshift. The vertical position of each halo on the plot is determined by $\log_{10}(1+z)$ at the redshift at which it exists, the horizontal positioning is arbitrary. The solid lines connect halos to their progenitors.

that between times t_1 and t_2 the group has split into smaller groups which we refer to here as "fragments".

We split such spuriously joined groups into one new group for each fragment which contains more than $N_{\rm min}$ of its constituent particles. Particles belonging to one of these fragments at time t_2 are assigned to the corresponding new group at time t_1. Particles belonging to no fragment, or to a fragment with fewer than $N_{\rm min}$ particles from the joined group, are assigned to the new group corresponding to the fragment "closest" to their position at time t_1. The separations used are weighted by a factor $M^{-1/3}$ to account for the spatial extent of the groups, where M is the mass of the fragment.

The splitting procedure is first carried out for halos at the penultimate time step and then repeated for each earlier output time in order of increasing redshift. For each time step a modified group catalogue is produced, which is then used to determine whether any halos at the previous time step need to be split. This ensures that if any bridge between a pair of halos persists for more than one time step the halos will be split at each time step where the bridge exists.

2.3 Mass Conservation

In the GALFORM semi-analytic model of Cole et al. (2000), halos may gain mass through mergers with other halos. In this model, the mass of a halo always increases with time, and the difference between the mass of a halo and the sum of the masses of its progenitors is due to the accretion of small, unresolved dark matter halos.

Here, we intend to replace the Monte-Carlo generated merger trees of the GALFORM model with merger trees derived from a simulation. These N-body merger trees may contain halos which decrease in mass from one time step to the next for the reasons described in Section 2.2 — the nature of the definition of a halo imposed by the FOF group finder and the possibility of disruption of halos by tidal forces. Consequently, a halo in a merger tree taken from a simulation may be somewhat *less* massive than its progenitors. In the GALFORM model this corresponds to the unphysical situation where a negative amount of mass is accreted in the form of sub-resolution halos.

Fig. 2 shows the distribution of the ratio $\mathrm{M_{prog}/M_{halo}}$, where $\mathrm{M_{halo}}$ is the mass of a halo and $\mathrm{M_{prog}}$ is the total mass of the immediate progenitors of the halo, which exist at the previous time step. If these merger trees had been created using the technique of Cole et al. (2000), then this ratio would always be less than one. It can be seen from the Fig. 2 that for halos less massive than about $10^{12} h^{-1}\mathrm{M}_{\odot}$ the total mass in the progenitors can exceed the mass of the halo they form at the next time step by up to 50%. Larger halos are less affected, but even the largest occasionally have progenitors with masses 5-10% greater than the mass of the halo.

Mass conservation can be forced on the N-body merger trees by simply adjusting the masses of some of the halos. Two opposite approaches to the problem are possible. Mass can be added to those halos which are less massive than their progenitors, or mass can be removed from the progenitors themselves. In order to show that the changes made to the halo masses have little effect on the semi-analytic model, we create merger trees using both methods.

Enforcing the conservation of mass in merger trees by adding mass is relatively straightforward. If a halo is less massive than its progenitors, its mass is increased to match that of the progenitors. The halo may, in turn, be a progenitor of a later halo which may now become less massive than its own progenitors. This later halo's mass will then also be increased. Changes made to halo masses at early times may therefore propagate to later times.

Similarly, if mass is removed from a halo to force conservation of mass, it may become less massive than its progenitors and reductions in mass could then propagate to earlier times. We attempt to remove mass in such a way as to minimize the effects on earlier halos. Each halo has a certain amount of "excess" mass beyond that of its progenitors, which was accreted over the last time step in the form of sub-resolution objects. This mass, if it exists, may be removed without the change propagating to earlier halos. When a halo which is less massive than its progenitors is found, mass is first removed from the excess mass of the largest progenitor. If still more mass must be removed, it is taken from the excess mass of the other progenitors in decreasing order of mass. If all of the excess mass of the progenitors is removed and yet more mass needs to be taken away, the masses of all of the progenitor halos are simply scaled down by a constant factor.

The algorithms described above are two opposite ways of dealing with the problem of mass conservation in the merger trees. While artificially altering the halo masses is clearly not ideal, if both methods produce similar results when the merger trees are fed into the semi-analytic model we can conclude that the changes we have made are not crucial. This comparison is carried out in Section 3.3.

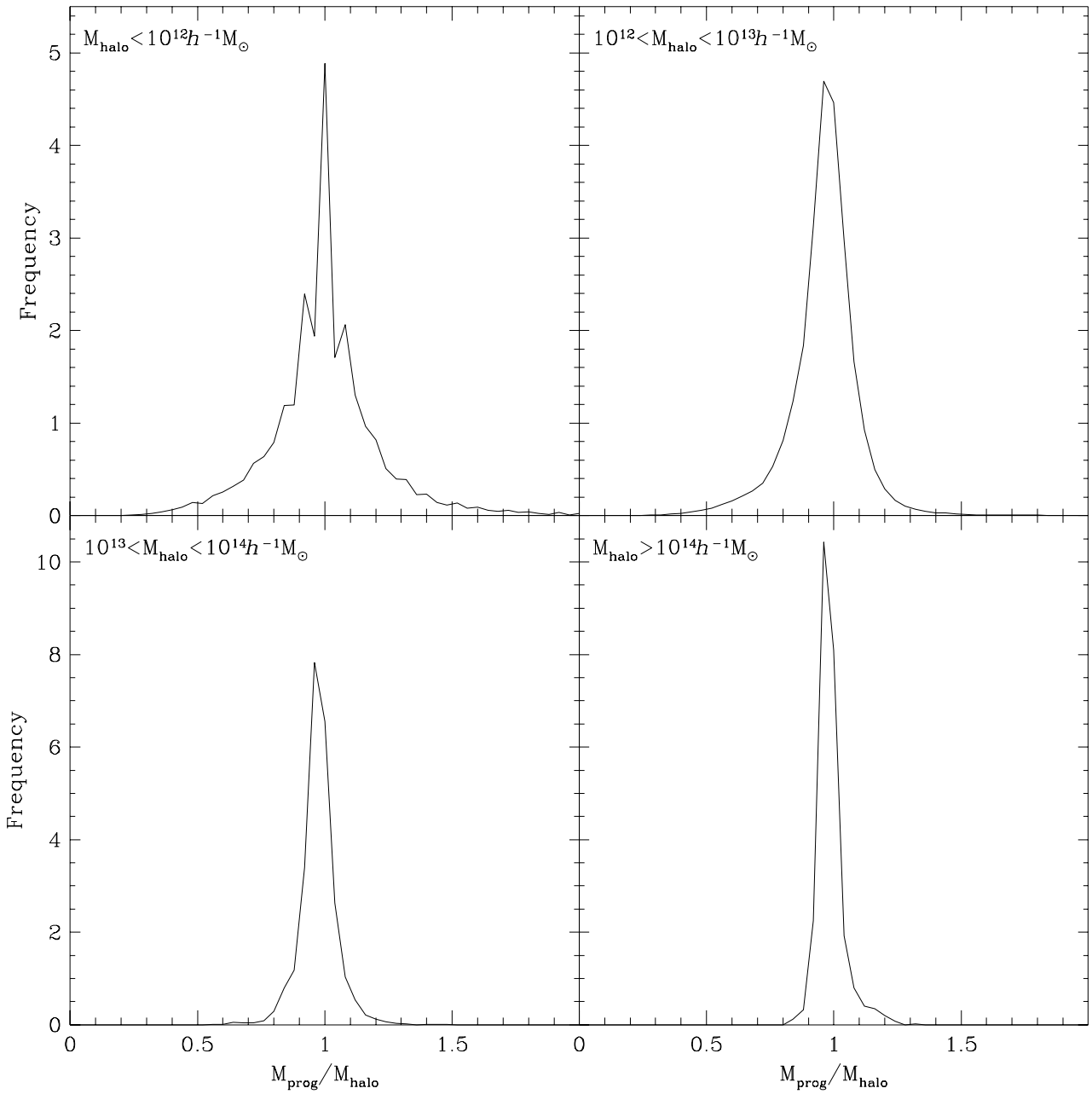

Figure 2. Distribution of the ratio of the mass of a progenitor of a halo, M_{prog}, to the mass of the halo at the next time step, M_{halo}. Each panel shows the distribution of M_{prog}/M_{halo} for halos in the mass range shown at the top of the panel.

3 COMPARISON BETWEEN GALFORM AND N-BODY GALFORM

In this section we describe our semi-analytic model, indicating how it differs from the model of Cole et al. (2000) on which it is based. We also explain how merger trees obtained from a simulation may be incorporated into the model.

3.1 The N-body GALFORM model

We use the GALFORM semi-analytic model to treat the process of galaxy formation within the dark matter halos in the GIF simulation. The model is described in detail by Cole et al. (2000) so here we present only a brief description of features that are important to this work. The original model of Cole et al. will be referred to as "standard GALFORM", and the version using merger trees taken from a simulation will be referred to as "N-body GALFORM".

The starting point for the standard GALFORM model is a set of merger trees created using a Monte-Carlo technique. The history of each halo is divided into a number of discrete time steps. Extended Press-Schechter theory is used to estimate the probability that a halo "fragments" into two progenitors when a step back in time of size δt is taken. The masses of the fragments are chosen at random from a distribution consistent with extended Press-Schechter theory. Halos are repeatedly split in this way to create merger trees. A mass resolution limit is imposed on the merger trees, below which progenitors are considered to be material acquired through continuous accretion. The mass resolution is normally set sufficiently low that the results of interest are not sensitive to its value. In the N-body GALFORM model, we replace these merger trees with those calculated directly from the GIF simulation as described in Section 2.2. The mass resolution limit is then determined by the mass of the smallest halo which can be resolved in the simulation.

The dark matter halos in the merger tree are assumed to be spherically symmetric with the radial density profile of Navarro, Frenk & White (1996; 1997):

$$\rho(r) \propto \frac{1}{r/r_{\rm NFW}(r/r_{\rm NFW}+1)^2}, \quad (1)$$

where $r_{\rm NFW}$ is the scale radius of the halo and is related to the concentration parameter, c, defined by Navarro, Frenk & White (1997) by $r_{\rm NFW} = r_{\rm virial}/c$, where $r_{\rm virial}$ is the virial radius of the halo.

Initially, the amount of gas in each halo is equal to the mass of the halo times the universal baryon fraction. This gas is assumed to be shock-heated to the virial temperature of the halo when it forms. The radial density profile of the gas is given by

$$\rho_{\rm gas}(r) \propto 1/(r^2 + r_{\rm core}^2), \quad (2)$$

where the core radius is given by $r_{\rm core}/r_{\rm NFW} \approx 1/3$ in accordance with the simulations of Navarro et al (1995). This core radius is allowed to grow with time from an initial value, $r_{\rm core}^0$, as gas is removed by cooling in order to maintain the same gas density at the virial radius. This ensures that the pressure at the virial radius, which would be maintained by shocks from infalling material, remains unchanged. In Section 4 we also consider a model with a core radius which is a fixed fraction of the scale radius.

To determine the rate at which gas can cool and form a disk at the centre of the halo, the cooling time of the gas is calculated as a function of radius using the cooling function of Sutherland & Dopita (1993). Gas which has had time to cool and fall to the centre of the halo is added to the disk where it is available to form stars.

When halos merge, the most massive galaxy becomes the central galaxy in the new halo. The resolution of the simulations used here is insufficient to follow the evolution of substructure within the dark matter halos. Instead, the dynamical friction time scale, as found by Lacey & Cole (1993), is used to determine when each satellite will merge on to the central galaxy. It should be noted at this point that the orbital parameters used to determine the dynamical friction time for each galaxy are assigned at random from a distribution consistent with the numerical results of Tormen (1997), even when using merger trees obtained from the simulation.

3.2 Parameters in the N-body GALFORM model

The GALFORM semi-analytic model requires a number of parameters to be specified, which can be divided into three categories. There are numerical parameters, parameters describing the background cosmology and parameters which describe the physical model of galaxy formation.

The numerical parameters are the mass resolution, $M_{\rm res}$, the number of time steps in the merger tree and the starting redshift. In the N-body GALFORM model these are all constrained by the properties of the simulation used to obtain the merger trees. The mass resolution is the mass of the smallest halo which our group finding algorithm can resolve, there is one time step for each simulation output and the starting redshift is the redshift of the first output. The cosmological parameters Ω_0, Λ_0, h, σ_8, Γ and, in the case of a simulation with a baryonic component, Ω_b are also determined by the simulation.

The remaining parameters allow us to vary the treatment of the processes involved in galaxy formation. In Section 4 we will vary several of these parameters in order to model the way in which gas cools and forms galaxies in the SPH simulation. The parameters we are interested in are:

- $r_{\rm core}$: the size of the core in the radial gas density profile, specified in terms of $r_{\rm NFW}$ (see eqn. 2).
- The evolution of $r_{\rm core}$ with time. $r_{\rm core}$ may be a fixed fraction of $r_{\rm NFW}$ or it may be allowed to increase with time as described in Section 3.1
- $f_{\rm df}$: The dynamical friction time scale for a satellite galaxy, which is used to determine when the galaxy merges with the central galaxy of the halo, is scaled by this factor. Consequently, increasing $f_{\rm df}$ reduces the rate at which galaxy mergers occur within halos. If star formation and feedback are neglected, as in the semi-analytic model of the SPH simulation which we describe in Section 4, this has no effect on the rate at which gas cools, but it does affect the distribution of galaxy masses in halos with more than one galaxy.

The other parameters in the model are the same as those in the reference model of Cole et al. (2000), with the

following changes due to the higher baryon density, $\Omega_b = 0.0377$, which we adopt here: $v_{\rm hot} = 250$km/s, $\alpha_* = -2.5$ and $f_{\rm ellip} = 0.5$.

Our prescription for star formation differs slightly from that of Cole et al. In our model, the time scale for star formation is given by

$$\tau_* = \tau_*^0 (V_{\rm disk}/200{\rm km\,s^{-1}})^{\alpha_*}, \quad (3)$$

where $V_{\rm disk}$ is the circular velocity of the galaxy disk and the time scale τ_*^0 is set to 3Gyr.

3.3 Effects of mass conservation

The upper panels of Fig. 3 show the galaxy luminosity functions in the b_J and K bands predicted by the N-body GALFORM model with the parameters of Section 3.2, using the two different methods described in Section 2.3 to enforce mass conservation in the merger trees. Over most of the luminosity range plotted, the two curves are essentially identical but there appear to be more galaxies at very faint b_J magnitudes when mass is removed from the merger trees. The majority of these galaxies formed in halos near the 10 particle ($\simeq 1.4 \times 10^{11} h^{-1} {\rm M}_\odot$) mass resolution limit imposed by the FOF group finder and their halos subsequently merged with other, larger dark matter halos. When mass conservation is enforced by removing mass from the merger trees (the dotted lines in Fig. 3) it is possible to end up with some halos with mass less than the resolution limit. The galaxies which form in them can have b_J band magnitudes around -14 or fainter. If instead mass is added to halos less massive than their progenitors, then the merger trees contain no halos with masses below the FOF resolution threshold and hence fewer faint galaxies.

These sub-resolution halos often exist in the merger trees of larger halos and could affect the evolution of larger, brighter galaxies. However, the agreement of the luminosity functions suggests that any effect is insignificant. The global star formation history and Tully-Fisher relation shown in the lower panels of Fig. 3 are similarly unaffected. (The extra point at the low luminosity end of the Tully-Fisher relation when mass is removed from the trees is also caused by the presence of sub-resolution halos which form very faint galaxies.)

Overall, the choice of method appears to make very little difference to the quantities plotted in Fig. 3, which suggests that the small amounts of mass being added to or removed from the merger trees do not significantly affect the properties of the resulting galaxies. The only region of the luminosity function which is affected is largely populated by galaxies which formed in halos with little or no resolved merger history, where the model cannot be expected to give reliable results. For the remainder of this paper we choose to enforce mass conservation by adding mass to the merger trees since this does not introduce halos with masses below the resolution limit.

3.4 Comparison with standard GALFORM

The mass resolution of the merger trees taken from the GIF simulation is equal to 10 particle masses or $1.4 \times 10^{11} h^{-1} {\rm M}_\odot$, i.e. $N_{\rm min} = 10$. This is much larger than the mass resolution $M_{\rm res} = 5.0 \times 10^9 h^{-1} {\rm M}_\odot$ used by Cole et al. (2000). This will clearly affect the properties of the galaxies predicted by the N-body GALFORM model, since gas will be unable to cool and start forming stars until lower redshifts where halos with masses greater than $M_{\rm res}$ have formed.

In order to investigate the effect of limited mass resolution on the N-body GALFORM model, we identify the different properties of the merger trees between standard and N-body GALFORM and use this knowledge to produce a modified version of the standard GALFORM model which reproduces the behaviour of the N-body GALFORM model. We can then increase the mass resolution of the merger trees in the modified model and observe the effects on the predicted galaxy properties.

There are three main reasons why the two models differ. Firstly, in the standard GALFORM model the mass resolution can be made arbitrarily small, whereas in the N-body model it is limited by the resolution of the simulation. Therefore we initially degrade the mass resolution of the standard GALFORM model to match that of the GIF simulation by setting the minimum halo mass, $M_{\rm res}$, equal to the mass of $(N_{\rm min} - 1)$ dark matter particles — any halo of this mass or less in the N-body simulation would not be identified by the FOF group finder and would not be included in the N-body merger trees.

Secondly, Jenkins et al. (2001) show that the Press & Schechter (1974) halo mass function used in the standard GALFORM model differs somewhat from the mass function determined from N-body simulations. We replace the Press-Schechter mass function in the standard GALFORM model with the mass function determined by Jenkins et al. This ensures that the distribution of halo masses at $z = 0$ in the standard GALFORM model matches the distribution in the simulation.

Finally, the distribution of progenitor masses for halos of a given mass predicted by the standard GALFORM model also differs from the distribution found in N-body simulations. Benson et al. (2001a) show that an empirical correction can be used to bring the progenitor mass distributions in the semi-analytic and N-body merger trees into closer agreement. The threshold linear overdensity for collapse from the spherical collapse model, δ_c, is replaced with an effective threshold $\delta_c^{\rm eff} = f_{\delta_c} \delta_c$. In the ΛCDM cosmology the following form for f_{δ_c} was found by Benson et al. to give reasonable agreement between the progenitor mass functions between redshifts 0 and 3:

$$f_{\delta_c} = 1 + 0.14[\log_{10}({\rm M_{halo}}/h^{-1}{\rm M}_\odot) - 15.64], \quad (4)$$

where $\rm M_{halo}$ is the mass of the final halo at redshift $z = 0$. This form of modification was suggested by Tormen (1998).

These modifications are intended to produce semi-analytic merger trees with statistical properties closely matched to those of the N-body merger trees. Fig. 4 shows the galaxy luminosity functions in the b_J and K bands, Tully-Fisher relations and global star formation histories for both the modified GALFORM model described above (dotted lines) and the N-body GALFORM model (dashed lines). It can be seen from the figure that these two models predict populations of galaxies with very similar statistical properties. The luminosity functions are in good agreement for K brighter than about -19 and b_j brighter than about -16. The

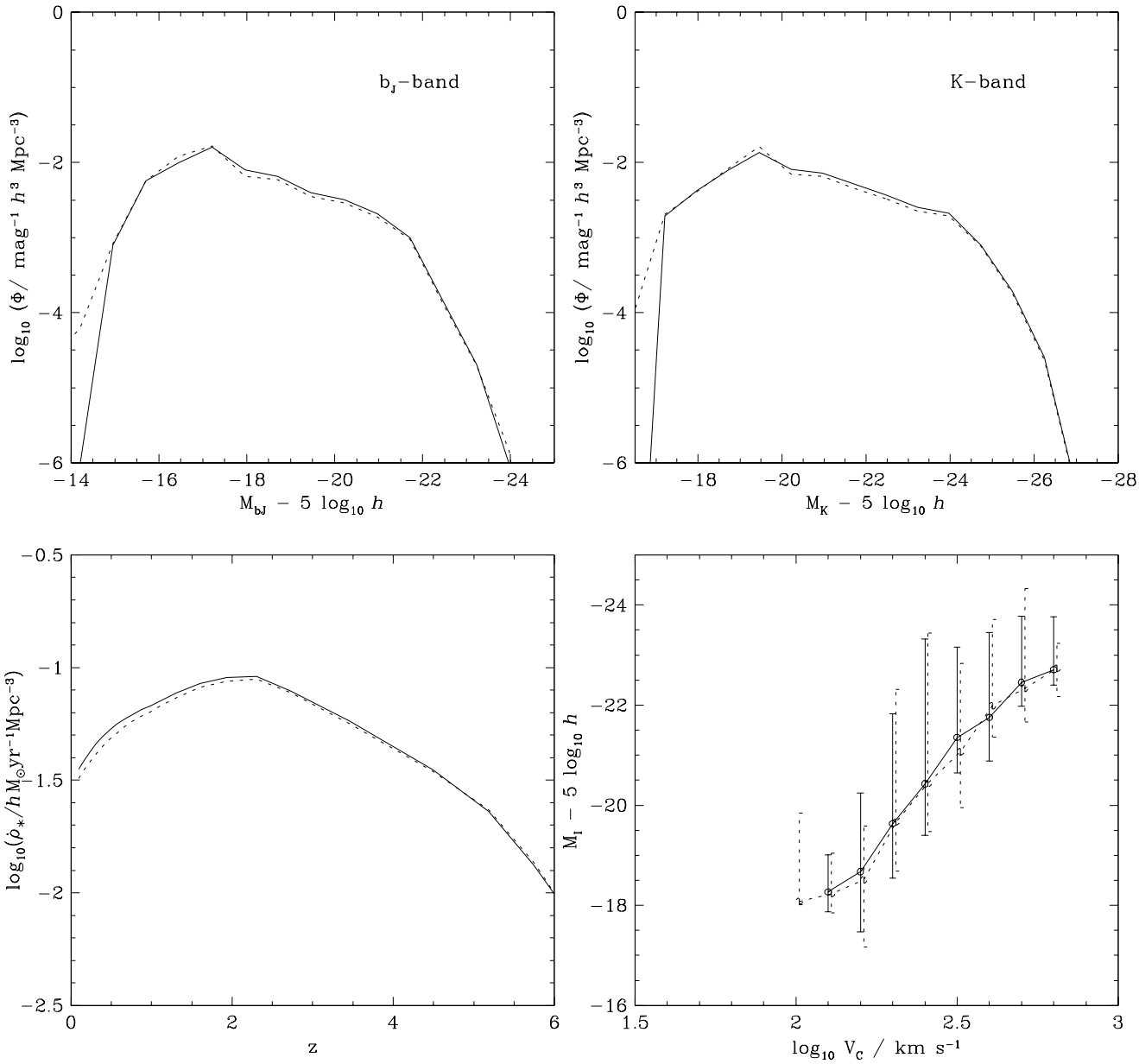

Figure 3. Luminosity functions, star formation histories and Tully-Fisher relations for galaxies predicted by the N-body GALFORM model using merger trees obtained from the GIF simulation with two different methods of enforcing mass conservation. The solid lines show results obtained when mass conservation in the merger trees is enforced by increasing the masses of halos less massive than their progenitors. The dotted lines show the results obtained if, instead, the masses of the progenitors of such halos are reduced.

Tully-Fisher relations and star formation histories are also in close agreement.

As pointed out previously, the fainter galaxies in these models occupy halos with very poorly resolved merger histories and their properties may be largely determined by the effects of limited mass resolution. The solid lines in Fig. 4 show the properties of the galaxies in the modified GALFORM model when the minimum halo mass $M_{\rm res}$ is reduced to $5.0\times10^9 h^{-1}{\rm M}_\odot$. This is much less massive than the smallest halo Benson et al. were able to resolve in their simulations and consequently, in this regime, eqn. (4) has not been tested and cannot be relied upon to produce a realistic distribution of progenitor masses. We therefore do not expect this model to reproduce the results of Cole et al. , and show it only to provide some indication of the magnitude of the effect of introducing low mass halos into the merger trees.

This "improvement" in mass resolution increases the number of faint galaxies, which form in small, previously unresolved halos. With a higher minimum halo mass the gas in these small halos is unable to cool until it becomes incorporated into objects more massive than $M_{\rm res}$. This is reflected in the luminosity functions which show that there are more bright galaxies and fewer faint galaxies at $z = 0$ in the model with poor mass resolution. The star formation history is consistent with this, showing that poor mass resolution results in reduced star formation at $z > 1$ and increased star formation at $z = 0$. However, calculating the global star formation rate involves a sum over all halos. At high redshifts this includes a large number of halos of low mass whose abundances are likely to be unrealistic due to our extrapolation of eqn. (4).

The effect on the Tully-Fisher plot of reducing $M_{\rm res}$ appears to be to reduce the luminosity of objects with a given circular velocity, by about 0.5 magnitudes in the I band at low circular velocities and by about 1 magnitude at high circular velocities. Again, this is expected if the enhanced resolution allows star formation at early times to reduce the amount of gas available for star formation at low redshift. Galaxies of all luminosities are affected which suggests that halos which are unresolved in the low resolution model play a noticeable part in the evolution of even the largest galaxies. Tests show that the relatively large scatter in the Tully Fisher relation in the N-body GALFORM model is due to the course time steps imposed by the number of simulation outputs available.

Overall, the predictions of the N-body GALFORM model closely match those of the standard GALFORM model when we take into account the differences in the halo mass function, the progenitor mass distribution and the mass resolution. The differences between the modified GALFORM models with high and low mass resolution indicate that the properties of the galaxies in the N-body model are affected to some extent by the resolution of the simulation. In order to attempt accurately to reproduce the properties of observed galaxy populations, an N-body simulation with significantly improved mass resolution would be required. This does not present a problem for our comparison between SPH and semi-analytic galaxy formation models because in both cases we use the same merger trees with the same mass resolution.

4 COMPARISON BETWEEN SPH AND N-BODY GALFORM

In this section we compare the results of an SPH simulation with the N-body GALFORM model, using merger trees derived from the dark matter component of the SPH simulation.

SPH is a Lagrangian numerical method which follows the motion of a set of gas elements represented by discrete particles. The thermal energy and velocity of each particle are known at any given time and each particle has a fixed mass. Properties of the gas at the position of a particle can be estimated by smoothing these quantities over the $N_{\rm SPH}$ nearest neighbouring particles. The gas properties are then used to calculate the forces acting on each particle in order to update the positions and velocities. In cosmological simulations both dark matter and gas particles are included and the particles are initially distributed in a manner consistent with a cosmological power spectrum. If the process of galaxy formation is to be simulated then radiative cooling of the gas must also be included.

The SPH simulation used here was performed using the Hydra code. This particular implementation includes a modification, described by Pearce et al. (2001), to prevent the rate of cooling of hot gas being artificially increased by nearby clumps of cold, dense gas, or "galaxies". Any gas hotter than 10^5K is assumed not to interact with gas at temperatures below 12 000K. Thus, for cooling purposes the density estimate for a hot particle near a galaxy is based only on the neighbouring hot particles and the cooling rate is unaffected by the presence of the galaxy.

The simulation has 80^3 gas and 80^3 dark matter particles with individual masses of $2.57 \times 10^9 h^{-1}{\rm M}_\odot$ and $2.37 \times 10^{10} h^{-1}{\rm M}_\odot$ respectively, contained in a cube of side $50h^{-1}$Mpc. The power spectrum is that appropriate to a cold dark matter universe with the following parameter values: mean mass density parameter $\Omega_0 = 0.35$, cosmological constant $\Lambda_0 = 0.65$, baryon density parameter $\Omega_b = 0.0377$, hubble constant $h = 0.71$, power spectrum shape parameter $\Gamma = 0.21$ and rms linear fluctuation amplitude $\sigma_8 = 0.90$. The gravitational softening length is $25h^{-1}$kpc, fixed in physical coordinates.

The metallicity of the gas in the simulation, measured in terms of the mass fraction of metals, Z, is uniform and varies linearly with time according to:

$$Z = 0.3 Z_\odot \, t(z)/t_0, \qquad (5)$$

where $Z_\odot$ denotes the solar metallicity, $t(z)$ is the age of the universe at redshift z and t_0 is the age of the universe at $z = 0$.

This simulation makes no attempt to treat star formation and does not include any prescription for stellar feedback, the re-heating of gas by energy released as a consequence of stellar evolution.

Fig. 5 shows the positions and masses of the galaxies which form in a $5h^{-1}$Mpc thick region in both the SPH simulation and N-body GALFORM implemented in the dark halos of the SPH simulation. The SPH "galaxies" shown here were identified using a FOF group finder on gas particles with temperatures between 8 000 and 12 000K (see Section 4.1.1).

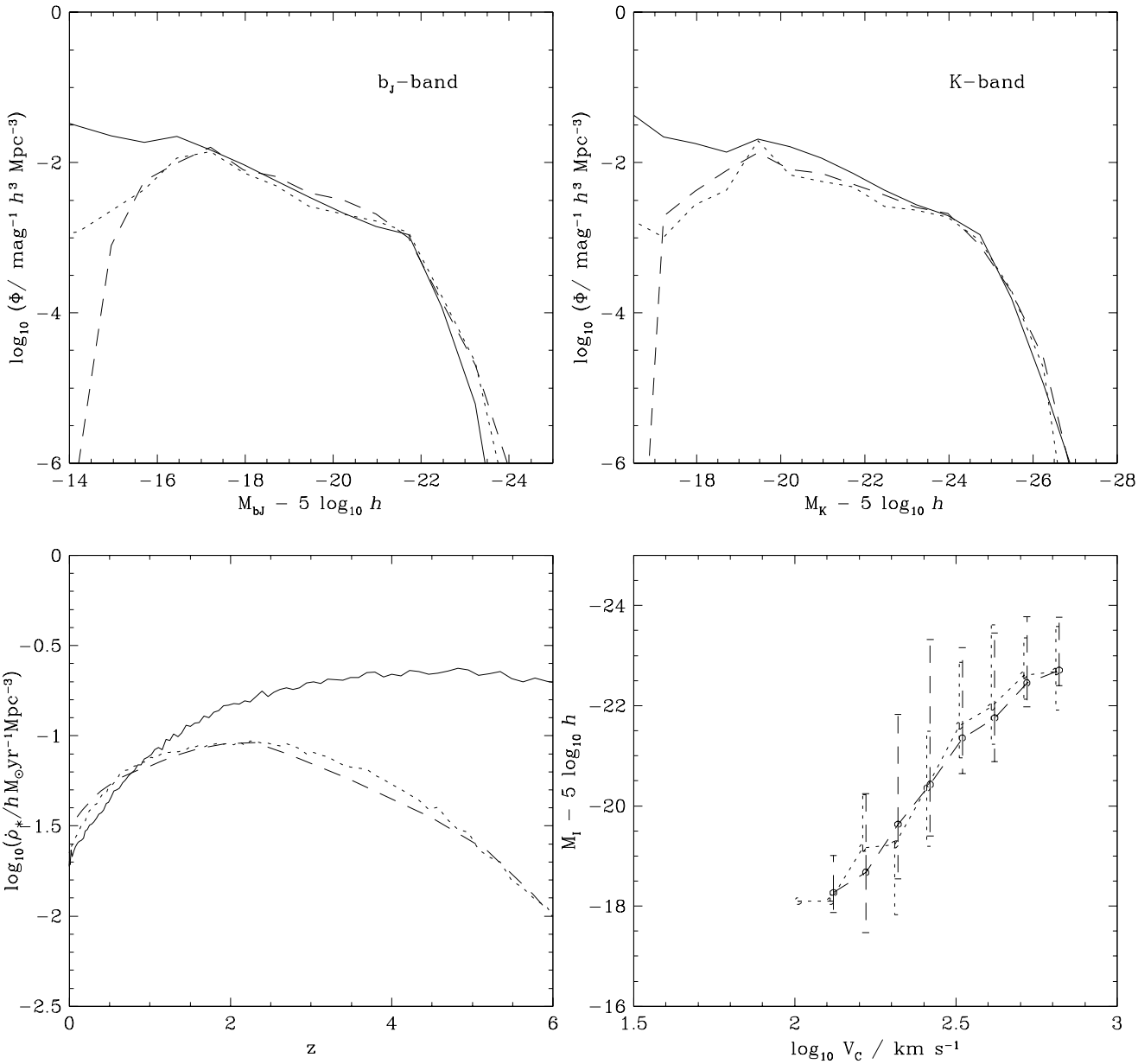

Figure 4. Luminosity functions, star formation histories and Tully-Fisher relations for three different models. The solid lines correspond to the GALFORM model using Monte Carlo generated merger trees as described by Cole et al. (2000), with the modifications explained in Section 3 and a mass resolution of $5 \times 10^9 h^{-1}\mathrm{M}_\odot$. The dotted lines show results from the same model with a mass resolution of $1.3 \times 10^{11} h^{-1}\mathrm{M}_\odot$, equivalent to that of the GIF simulation. The dashed lines show results obtained from the N-body GALFORM model which uses merger trees derived from the simulation.

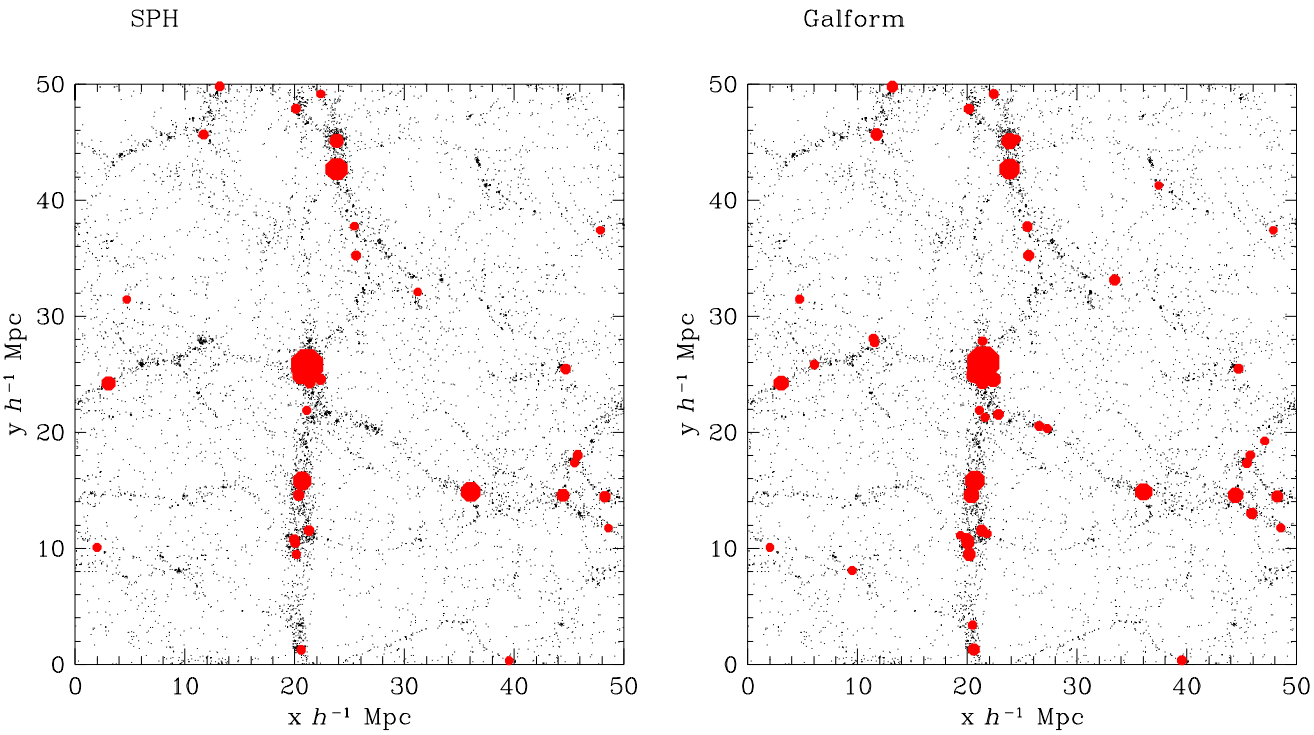

Figure 5. Positions and masses of galaxies in a $5h^{-1}$Mpc thick slice through the simulation volume. The panel on the left shows galaxies found in the SPH simulation using a friends of friends algorithm to identify clumps of cold gas particles. The panel on the right shows the galaxies predicted by the N-body GALFORM model. Each circle represents a galaxy, the area being proportional to the mass of the galaxy. Dark matter particles are shown as dots. Only galaxies with masses greater than 32 gas particle masses, or $8.2 \times 10^{10} h^{-1} \mathrm{M}_{\odot}$, are shown.

4.1 Modelling SPH with N-body GALFORM

In order to produce a semi-analytic model of the SPH gas simulation using N-body GALFORM we first remove the treatment of star formation, feedback and chemical enrichment from GALFORM. We set the metallicity of the gas to be the same as that in the simulation, using eqn. (5).

The cooling rate of the gas in our simulation depends on its density, which is estimated by searching for the $N_{\rm SPH}$ nearest neighbours. The density of gas in halos with less than $N_{\rm SPH} = 32$ gas particles, or a total gas mass less than $8.2 \times 10^{10} h^{-1} \mathrm{M}_{\odot}$, will therefore be severely underestimated and cooling will be suppressed. Consequently, the mass of gas which cools is dependent on the particle mass.

In order to model this effect in the semi-analytic treatment, we first investigate the variation of the mean estimated density of gas in halos in the SPH simulation with halo mass. A characteristic volume for each gas particle can be obtained by dividing its mass by its SPH density estimate. The total volume of the gas in a halo is calculated by summing the volumes of its constituent gas particles. The total volume is then divided by the mass of gas in the halo to obtain an estimate of the mean gas density. Fig. 6 shows this density estimate plotted against halo mass, at redshift $z = 0$. In halos identified using the FOF group finder with $b = 0.2$ we expect the mean gas density to be several hundred times the universal mean gas density. The dotted line shows the median of the mean densities of halos of a given mass. Halos with more than 32 particles have approximately constant mean density, although the density does increase somewhat with halo mass.

The estimated density rapidly drops once the halo mass falls below 32 dark matter particle masses. Since the cooling time of the gas is inversely proportional to its density this could significantly affect the amount of gas which cools in the smaller halos in the simulation. We incorporate this effect into the semi-analytic model by increasing the cooling time for gas in halos of fewer than 32 particles. A least squares fit to Fig. 6 gives:

$$\log_{10} \frac{\bar{\rho}_{\rm SPH}}{\rho_{\rm crit} \Omega_b} = 1.23 \log_{10} \mathrm{M}_{\rm halo} - 11.79, \qquad (6)$$

where $\bar{\rho}_{\rm SPH}$ is the mean gas density estimated from the SPH simulation and $\mathrm{M}_{\rm halo}$ is the mass of the halo. The cooling time in our model is inversely proportional to the mean density of the gas in the halo. In halos of fewer than 32 particles we replace the cooling time, $\tau_{\rm cool}$, with a longer cooling time, $\tau_{\rm cool}^{\rm SPH}$, given by

$$\tau_{\rm cool}^{\rm SPH} = k \, \tau_{\rm cool} \frac{\Omega_b \, \rho_{\rm crit}}{\bar{\rho}_{\rm SPH}}, \qquad (7)$$

where $\rho_{\rm crit}$ is the critical density. We set the constant of proportionality, k, in this relation by requiring that the cooling time for halos of 32 particles is unchanged.

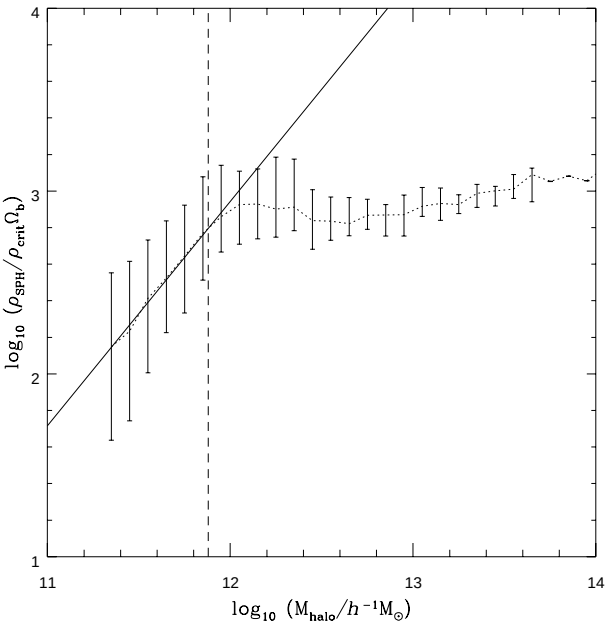

Figure 6. Mean halo gas density $\rho_{\rm SPH}$ plotted against halo mass $M_{\rm halo}$ at redshift $z = 0$. The density is expressed in terms of the critical density $\rho_{\rm crit}$ multiplied by the baryon fraction. The mean density is calculated from density estimates for individual particles in the SPH simulation. The dotted line shows the median of the mean halo gas densities as a function of halo mass. The error bars show 10 and 90 percentile limits. The vertical dashed line is at a halo mass corresponding to 32 dark matter particles. The solid line is a power law fit to the median density for halos of fewer than 32 particles.

4.1.1 Halo by halo comparison

The masses of individual galaxies in the N-body GALFORM model depend on the rate at which galaxy mergers occur. Since the merger rate in the SPH simulation may not be the same as that in the semi-analytic model, we first compare the total amount of gas which cools in halos of a given mass. This quantity should be independent of the merger rate, at least in the semi-analytic case, and can be used to compare the treatment of cooling in the two models. In the SPH simulation a large galaxy forming at the centre of a halo through mergers may gravitationally affect the density, and hence the cooling rate, of nearby gas, but we do not expect this to be a large effect and the mass of gas which cools should be only weakly dependent on the merger rate.

We adopt two different models for the evolution of the gas density profile. The first is that used by Cole et al. (2000) in which the core radius in the gas profile is allowed to increase with time in order to maintain the gas density at the virial radius. We may vary the initial core radius, $r^0_{\rm core}$, in order to adjust the amount of gas which cools. The second is a simpler model in which the core radius remains a constant fraction of the halo scale radius, $r_{\rm NFW}$. Again, the size of this fixed core may be varied in order to adjust the rate at which cooling occurs.

In order to quantify the mass of cold gas present in halos in the SPH simulation, we first associate gas particles with dark matter halos. A gas particle is considered to belong to a halo if it lies within a linking length $b = 0.2$ of a dark matter particle which belongs to that halo. In the unlikely event that dark matter particles from more than one halo are found within the linking length the gas particle is assigned to the halo containing the nearest dark matter particle. The linking length used in this procedure is the same as that used to identify dark matter halos with the FOF group finder. This ensures that the condition for a gas particle to be associated with a halo is consistent with the definition of halo membership used for the dark matter particles.

The cooling function in our simulation permits gas to cool only to a temperature of 10^4K. This allows us to distinguish between gas which has been heated and has subsequently cooled to 10^4K and the diffuse cold gas in voids which has never been heated and is at much lower temperatures. The mass of gas which has cooled in each halo is obtained by summing the masses of all gas particles associated with the halo with temperatures between 8 000K and 12 000K. In the N-body GALFORM model, the amount of cold gas in each halo is simply the mass of gas which has cooled from the hot phase, since the model includes no star formation.

Fig. 7 shows the mean fraction of gas which has cooled as a function of halo mass, in both N-body GALFORM and the SPH simulation. Here we consider four different N-body GALFORM models. We vary the initial core radius in the gas profile between $r^0_{\rm core} = 1.0 r_{\rm NFW}$ and $0.15 r_{\rm NFW}$ and either fix the core radius as a fraction of the NFW scale radius or allow it to increase with time as described earlier. In the case of a fixed core, $r_{\rm core} = r^0_{\rm core}$ at all times.

The dotted lines in Fig. 7 show N-body GALFORM models which include the modification to the cooling time in low mass halos described by eqn. (7). All four models reproduce the quantities of cold gas observed at redshift $z = 0$ in the SPH simulation remarkably well, for halos of mass greater than about $10^{12} h^{-1}{\rm M}_\odot$ or around 40 dark matter particles — even in the worst case the difference is less than 50%. We find that if the core radius in the gas density profile is allowed to increase as gas cools, a small initial value, $r^0_{\rm core} = 0.15 r_{\rm NFW}$, is required to match the fraction of cold gas in the simulation. If the core radius is fixed as a fraction of the NFW scale radius a much larger value, $r^0_{\rm core} = 1.0 r_{\rm NFW}$, is necessary.

The dashed lines in the figure show the fraction of gas which cools if cooling is allowed to occur at the normal rate in halos of all masses down to the mass of the smallest halo we can resolve in the simulation. Surprisingly, this appears to have little effect on halos with fewer than 32 dark matter particles for which the cooling rate has been altered. The fraction of gas which has cooled in larger halos also increases by a similar amount. The extra cold gas in these halos must have cooled in progenitors of fewer than 32 particles before being incorporated into larger halos. Overall, the change is not large, with some halos having around 10-20% more cold gas on average. This suggests that our results are not particularly sensitive to the way in which we model the loss of cooling efficiency in small halos, although in both cases the agreement between the SPH simulation and the semi-analytic model is poor in such halos.

Fig. 8 shows a direct comparison between the masses of cold gas in individual halos in the SPH simulation and the four N-body GALFORM models of Fig. 7, again using

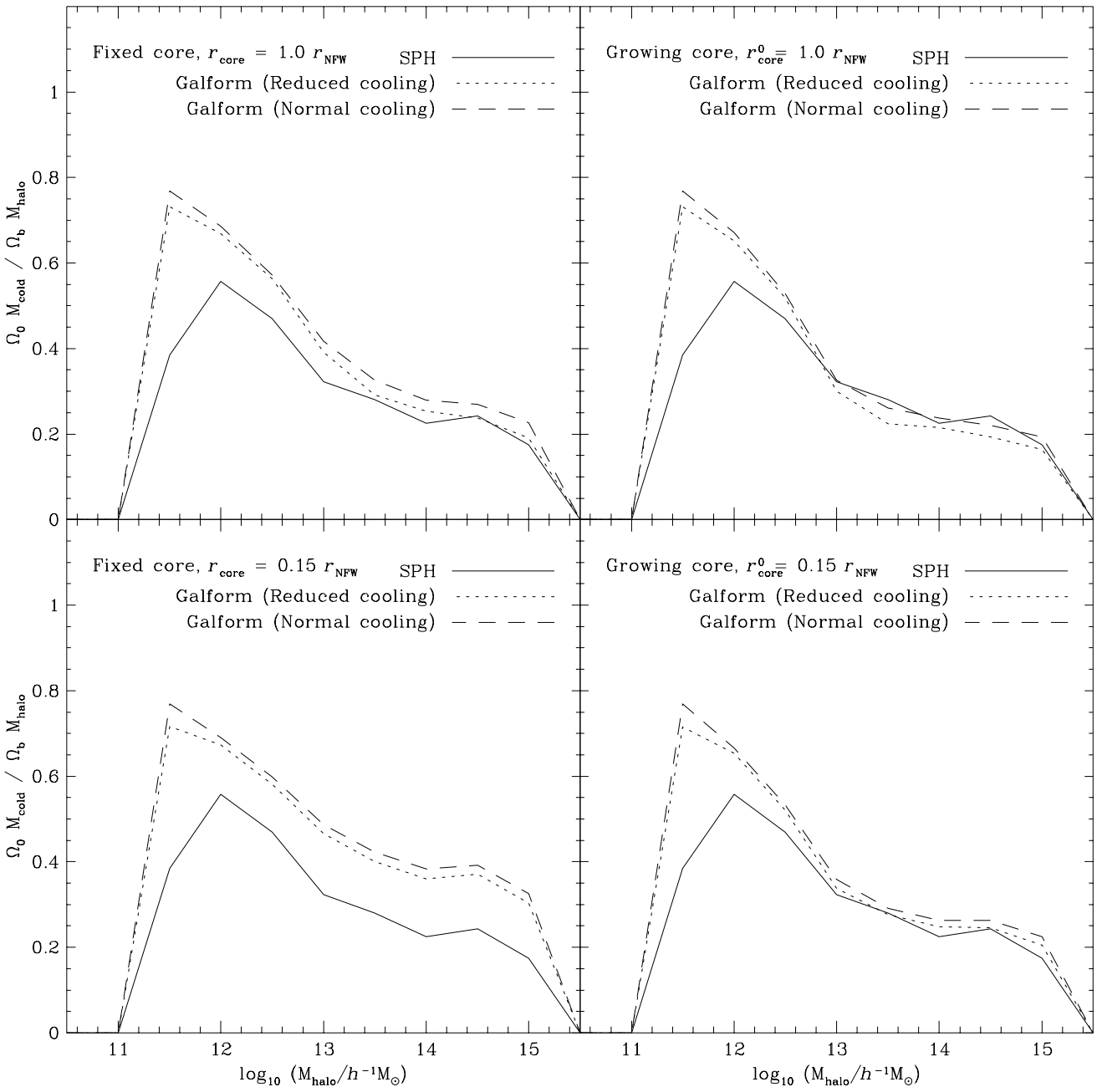

Figure 7. Mean fraction of halo gas which has cooled at redshift $z = 0$ as a function of halo mass. The solid lines show the mean cooled gas fraction in halos in the SPH simulation and are the same in all four panels. The dotted lines show the cold gas fraction in N-body GALFORM models where the cooling time in low mass halos is increased according to eqn (7). The dashed lines show N-body GALFORM models without this adjustment. In the upper panels the initial core radius is set equal to the NFW scale radius of the halo. In the lower panels the core radius is set to 0.15 times the scale radius. In the panels on the left hand side the core radius remains fixed at its initial value for all redshifts, in the panels on the right it is allowed to increase to maintain the density of gas at the virial radius.

the modified cooling time for low mass halos. The mass of cold gas predicted by N-body GALFORM is plotted against the mass of cold gas in the simulation for each halo, with the initial core radius set to $r_{\rm NFW}$ in the upper panels and $0.15r_{\rm NFW}$ in the lower panels. In the models shown on the left-hand side the core radius remains fixed at its initial value at all times. The solid lines show where the points would lie if the simulation and the semi-analytic models were in perfect agreement.

Again, in all four cases the mass of cold gas in the SPH simulation is well correlated with the mass of cold gas in the N-body GALFORM model. The small scatter, at least at high masses, shows that the dependence of cold gas mass on merger history must be similar in the SPH simulation and the semi-analytic model. N-body GALFORM with a gas density profile with a fixed core radius appears to cool on average more gas in halos of all masses than the SPH simulation. This can be alleviated to some extent by increasing the size of the core in the gas profile but it appears that a rather large core in the gas distribution would be required to obtain good agreement. Allowing the core radius to increase as gas cools reduces the rate of cooling and results in closer agreement with the simulation; the best agreement is obtained for a small initial core radius of around $0.15r_{\rm NFW}$, although the mass of cold gas in each halo is clearly not particularly sensitive to the initial core radius in this GALFORM model.

Fig. 9 shows the mass of cold gas in progenitors of four of the larger halos in the simulation as a function of redshift. The mass of cold gas in the simulation (solid lines) at a given redshift is obtained by summing the masses of all cold gas particles associated with the progenitors of the final halo at that redshift. Particles are associated with halos using the method described earlier in this section and, as before, "cold" particles are those with temperatures of 8 000–12 000K. Similarly, the mass of cold gas in the N-body GALFORM model is obtained by summing the masses of the galaxies in the progenitor halos. Here we show results for two models, one with $r_{\rm core}$ fixed at $r^0_{\rm core} = 1.0r_{\rm NFW}$ (dotted lines) and the other with a growing core which has an initial core radius $r^0_{\rm core} = 0.15r_{\rm NFW}$ (dashed lines). The model of Cole et al. used a gas profile with a larger initial core radius, $r^0_{\rm core} = 0.33r_{\rm NFW}$.

The long dashed lines show the mass of cold gas in progenitors in the simulation if instead of associating gas particles with halos directly, we use the FOF group finder to first identify clumps of cold gas and then associate clumps with dark matter halos. A clump is assigned to a halo if a dark matter particle from that halo is found within a dark matter linking length of the clump's centre of mass. If particles belonging to several halos are found in this region, the nearest to the centre of mass is used. A linking length $b = 0.02$ is used to identify the clumps and a minimum group size of 10 particles is imposed on the clumps. These lines are shown in Fig. 9 only to illustrate that there is some dependence on the way in which we define "cold gas" in the simulation. This second method will certainly underestimate the mass of cold gas because the group finder imposes a minimum mass on the clumps, missing smaller groups of cold particles. Also, at high redshift the gravitational softening length exceeds the linking length used to identify the clumps, so particles which ought to be considered part of a clump may not have collapsed to sufficiently high densities to be picked up by the group finder. We find that most of the discrepancy between these two SPH results is due to cold particles in small groups of fewer than five particles, at least with $b = 0.02$.

It is also possible that the first method of counting individual gas particles associated with halos overestimates the mass of cold gas in smaller halos, where the linking length becomes a significant fraction of the radius of the halo. Any particle within a linking length of the outer dark matter particles of the halo may be associated with that halo. Despite this uncertainty, it appears that more of the cold gas found in the simulation cooled at high redshift than in either of the N-body GALFORM cases considered. At redshift 2 the discrepancy is approximately a factor of 2. Allowing the core radius to increase from a small initial value helps somewhat by encouraging more cooling initially and slightly suppressing it later, but the improvement is small compared to the size of the discrepancy with the SPH simulation for redshifts greater than around 2. Reducing the initial core radius in this model further has little effect on these results.

The dotted and dashed lines in Fig. 7 compare N-body GALFORM models with and without an increased cooling time for small halos (eqn. 7), which is intended to mimic the effects of the SPH smoothing algorithm on small, isolated groups of gas particles. The fraction of gas that has cooled in the smallest halos appears to be unaffected by this change, which suggests that the cooling rate in halos at or just below our mass resolution is not drastically reduced. We have tried to model the effect of limited resolution on cooling in SPH blobs of fewer than 32 dark matter particles, but in the N-body GALFORM model no cooling is possible in halos of fewer than 10 dark matter particles. It appears that in our SPH simulation some cooling *does* occur in these halos. However, it may not be useful to model the rate of cooling in this regime, since it is entirely artificial and likely to be dependent on the details of the SPH implementation employed. In any case, when halos in the SPH simulation first grow to 10 dark matter particles they may have already cooled some gas. These halos will eventually be incorporated into larger halos, where the cold gas mass becomes dominated by material which cooled in well resolved halos so that at late times the SPH and GALFORM calculations converge.

4.1.2 Galaxy by galaxy comparison

Fig. 10 shows the number density of galaxies as a function of mass in the SPH simulation and in the N-body GALFORM model at redshift $z = 0$. Here, SPH "galaxies" are groups of particles identified by the FOF group finder applied to all particles with temperatures in the range 8 000–12 000K. We use a linking length $b = 0.02$ and impose a minimum group size of 10 particles. Two N-body GALFORM cases are shown, one with a core of fixed size $r_{\rm core} = r_{\rm NFW}$ in the gas density profile, the other with a growing core of initial size $r^0_{\rm core} = 0.15r_{\rm NFW}$. In both cases N-body GALFORM predicts about 50% more galaxies with masses around $3\times10^{11}h^{-1}{\rm M}_\odot$ or less and fewer galaxies with masses greater than this. The deficit in the number of massive galaxies is most apparent in the model with a large, fixed gas core radius. Since we know that the total amount of gas cooled in the semi-analytic models in each halo is similar to the amount that cooled in

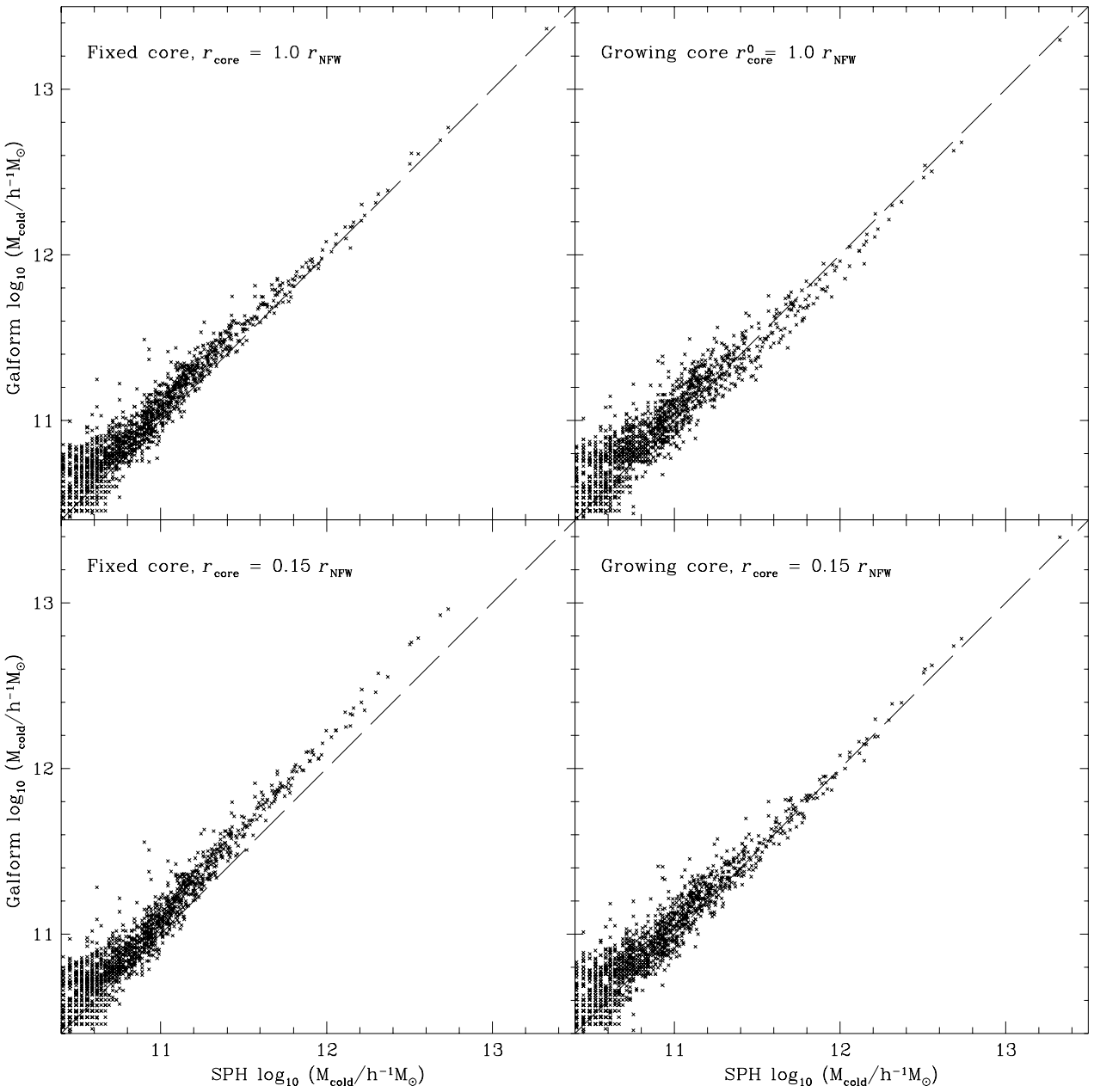

Figure 8. Halo cold gas mass, $M_{\rm cold}$, in four different N-body GALFORM models plotted against Halo cold gas mass in the SPH simulation at redshift $z = 0$. Each point corresponds to a single dark matter halo. The upper panels show N-body GALFORM models with $r^0_{\rm core} = 1.0 r_{\rm NFW}$. The lower panels have $r^0_{\rm core} = 0.15 r_{\rm NFW}$. In the panels on the left, the core radius in the gas density profile is a fixed fraction of the NFW scale radius. In the panels on the right the core radius is allowed to grow in order to maintain the gas density at the virial radius.

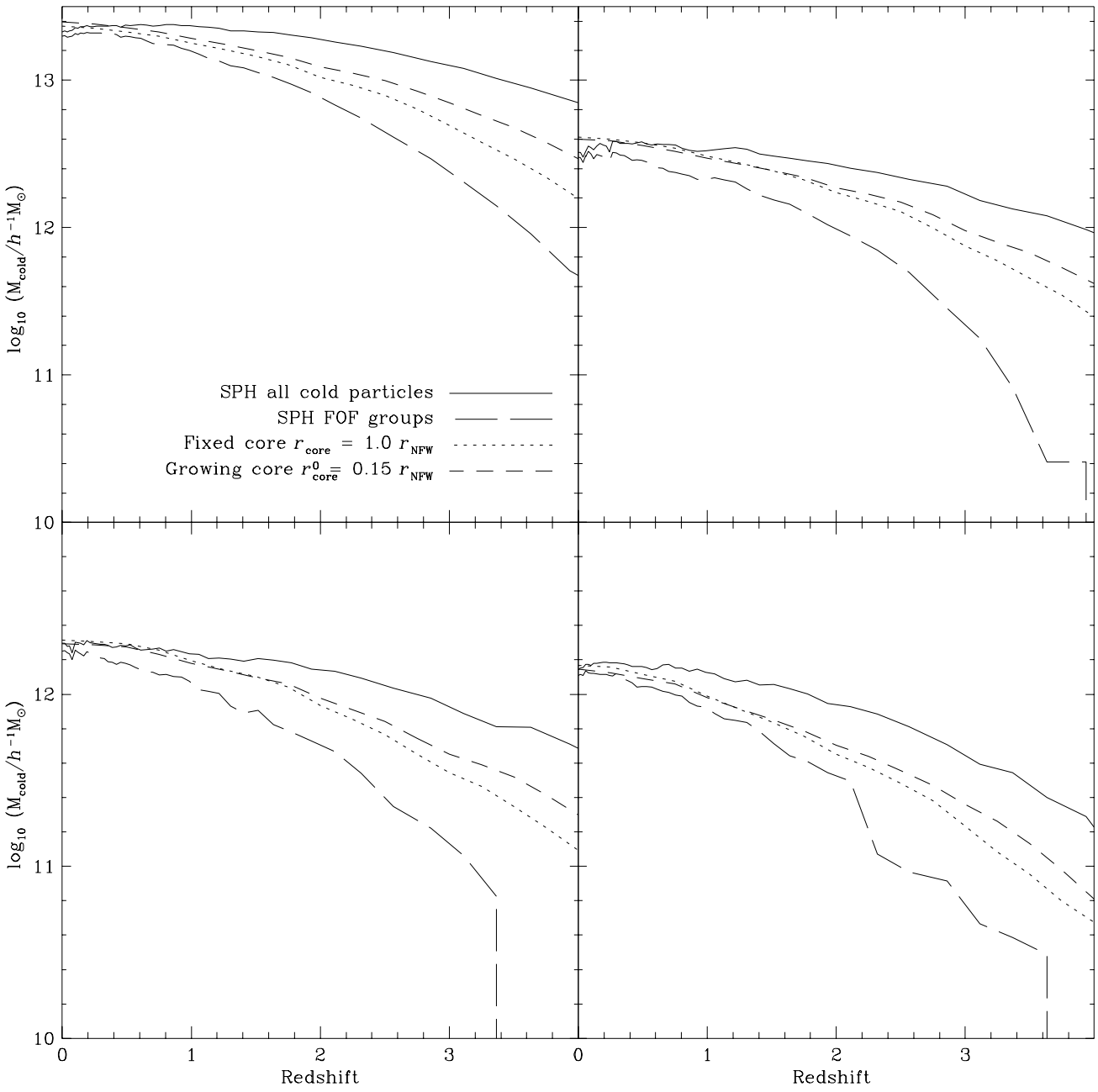

Figure 9. Mass of cold gas in the progenitors of four halos as a function of redshift. Each panel corresponds to a single halo at $z = 0$. The solid line shows the mass of cold gas in the SPH simulation obtained by summing the masses of all cold gas particles in the progenitors. The long dashed line shows the mass of cold gas obtained by summing the masses of all FOF groups of cold particles in the progenitors. The dotted lines correspond to an N-body GALFORM model with a fixed core radius in the gas density profile with $r_{\rm core} = r_{\rm NFW}$. The short dashed lines correspond to a model with a growing core radius of initial value $r^0_{\rm core} = 0.15 r_{\rm NFW}$

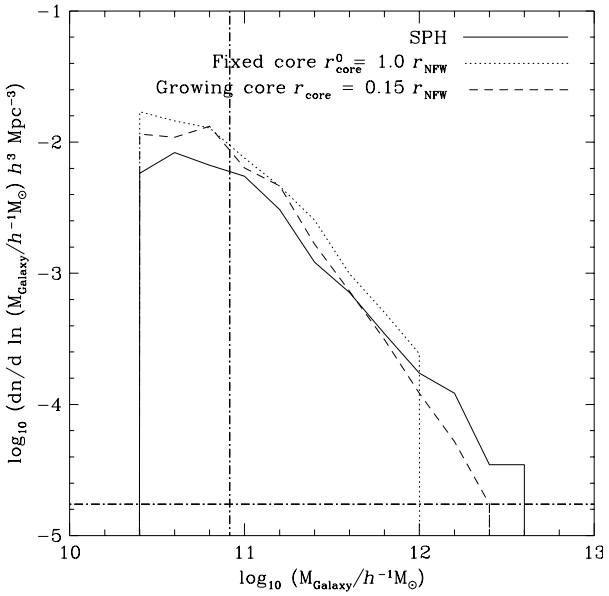

Figure 10. Galaxy number density as a function of cold gas mass at redshift $z = 0$. The solid line shows galaxy number density in the SPH simulation. The other lines correspond to N-body GALFORM models with 1) a fixed core radius $r_{\rm core} = r_{\rm NFW}$ (dotted line) and 2) a growing core which initially has $r^0_{\rm core} = 0.15 r_{\rm NFW}$ (dashed line). The horizontal dot-dashed line shows the number density equal to one object per simulation volume. The vertical dot-dashed line is at a mass equal to 32 gas particle masses.

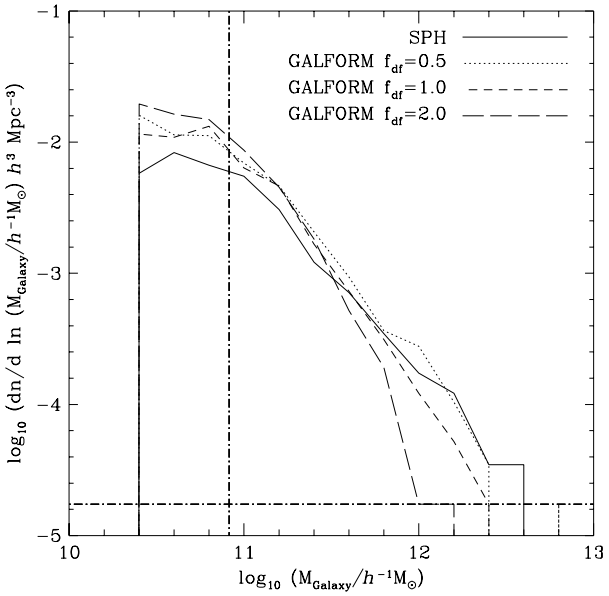

Figure 11. Galaxy number density as a function of cold gas mass at redshift $z = 0$ for N-body GALFORM models with three different merger rates. All three models have gas profiles with a growing core radius which is initially set to $r^0_{\rm core} = 0.15 r_{\rm NFW}$. The merger time scale parameter $f_{\rm df}$ is varied between 0.5 (dotted line), 1.0 (short dashed line) and 2.0 (long dashed line). The solid line shows the galaxy number density in the SPH simulation and is identical to the solid line in Fig. 10. The horizontal dot-dashed line shows the number density corresponding to one object per simulation volume. The vertical dot-dashed line is at a mass equal to 32 gas particle masses. The curves are truncated at 10 gas particle masses.

the simulation (see Fig. 8), this suggests that there is more merging occurring in the simulation. This does not necessarily indicate a failure of the semi-analytic model, however, since it is likely that numerical effects in the simulation contribute significantly to the merger rate.

To test this hypothesis, we vary the merger time scale parameter, $f_{\rm df}$ in the semi-analytic models. Fig. 11 shows galaxy number density as a function of mass for three N-body GALFORM models with $f_{\rm df} = 0.5$, 1.0 and 2.0. All three have gas profiles with growing cores of initial radius $r^0_{\rm core} = 0.15 r_{\rm NFW}$. Doubling the merger time scale ($f_{\rm df} = 2.0$) drastically reduces the number of more massive galaxies and prevents the formation of any galaxies more massive than $10^{12} h^{-1} {\rm M}_\odot$. Halving the merger time scale ($f_{\rm df} = 0.5$) improves agreement with the simulation by increasing the masses of the largest galaxies and reducing the number of small galaxies. However, the improvement is relatively small and, in any case, the treatment of mergers in the N-body GALFORM model reproduces distribution of masses observed in the simulation reasonably well with our default $f_{\rm df} = 1.0$.

The N-body GALFORM model described in Section 4 does not allow semi-analytic galaxies to be compared with their SPH counterparts on a one to one basis because mergers between galaxies in N-body GALFORM are treated in a statistical manner. While the agreement between the galaxy mass distributions suggests that the overall merger rate in the N-body GALFORM model is similar to that seen in the simulation, we cannot expect mergers to occur between the same galaxies in the two cases, and hence it is not possible to identify clumps of cold gas particles with individual semi-analytic galaxies.

This problem could be avoided by following the substructure within dark matter halos to determine when mergers between galaxies occur, using a method similar to that of Springel, White, Tormen & Kauffmann (2001). Unfortunately the halos in our simulation typically contain too few particles for this to be practical. Any dark matter substructure will rapidly be destroyed by numerical effects.

In order to compare the masses of individual galaxies directly, we need an alternative way to ensure that the same galaxies merge in each model. We do this by using information from the baryonic component of the SPH simulation to merge N-body GALFORM galaxies. We first populate the simulation volume with galaxies calculated using the N-body GALFORM model, with merging of galaxies completely suppressed. We find the halo in which each semi-analytic galaxy first formed, and identify the gas particles associated with that halo as those with indices corresponding to the indices of the dark matter particles in the halo — this is possible because in our SPH simulation gas and dark matter particles with the same indicies are initially at the same locations and tend to remain in the same halos at later times. By redshift $z = 0$ some of these particles will be contained within SPH galaxies. Each semi-analytic galaxy is assigned to the SPH galaxy wich contains the largest number of gas particles from the halo in which it formed. This procedure often results in

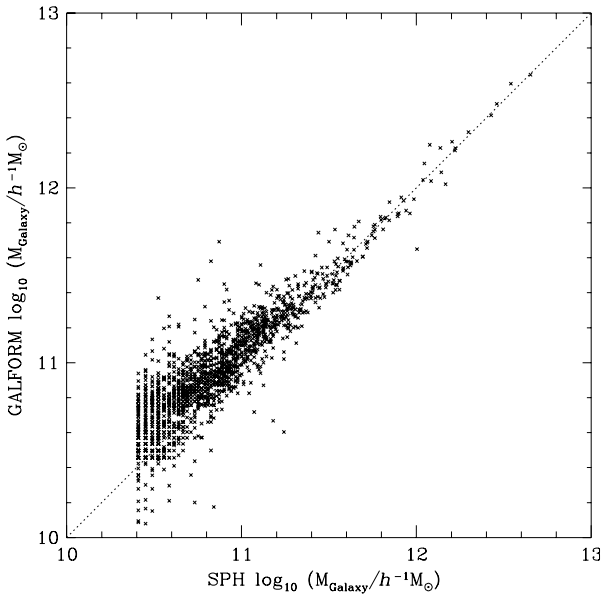

Figure 12. Comparison between galaxy masses in the SPH and N-body GALFORM models. The merger scheme described in Section 4.1.2 is used to identify N-body GALFORM galaxies with SPH galaxies. Galaxies lying on the dotted line have equal masses in both models.

several semi-analytic galaxies being assigned to the same blob of cold gas at redshift $z = 0$. These galaxies are assumed to have merged and their masses are added together. It is possible to think of rare situations where our method might incorrectly merge galaxies, but this is the best that can be done within the limitations of the SPH simulation.

We are only able to detect SPH galaxies with 10 particles or more, so it is inevitable that sometimes a semi-analytic galaxy will not be assigned to any SPH galaxy. This would occur if the semi-analytic galaxy formed in a halo which, in the simulation, failed to cool enough particles to constitute a group by redshift $z = 0$. Such galaxies are generally found in small, recently formed halos and typically have masses of around 10 gas particle masses or less. These galaxies account for about 20% of the total semi-analytic galactic mass in the simulation volume.

Since the unmatched semi-analytic galaxies largely correspond to SPH galaxies which have yet to gain enough cold particles to be identified by the group finder, we simply omit them from the comparison shown in Fig. 12. Here, we compare the masses of the merged semi-analytic galaxies with the corresponding galaxies in the SPH simulation. Each point on the plot represents a single SPH galaxy which has been associated with one or more semi-analytic galaxies. There is clearly a very strong correlation between the mass of each simulated galaxy and its semi-analytic counterpart, although the N-body GALFORM galaxies appear to be systematically more massive by up to 25% at low masses. The scatter in this plot is comparable to that in Fig. 8. There are a few outlying points which may correspond to cases where our algorithm has assigned N-body GALFORM galaxies to the wrong SPH galaxy.

Finally, we compare the clustering of galaxies in the two models. While the spatial distribution of dark matter halos in the N-body GALFORM model is identical to that in the simulation, the number of galaxies in each halo and their distribution within the halo may differ. Fig. 13 shows two point galaxy correlation functions for galaxies in the SPH simulation and two different N-body GALFORM models, both of which have gas profiles with growing core radii which are initially set to $r^0_{\rm core} = 0.15 r_{\rm NFW}$. In the first GALFORM model, merging between galaxies is treated using the dynamical friction approach of Cole et al. with $f_{\rm df} = 0.5$, which gives a closer match to the distribution of galaxy masses in the simulation than our default value of 1.0 (see Fig. 11.) In the second GALFORM model, we use the SPH based merging scheme described earlier in this section and put each merged GALFORM galaxy at the position of its associated SPH galaxy. In each case, we include only the 700 (left panel of Fig. 13) or 300 (right panel) most massive galaxies in our calculation. This ensures that the overall density of galaxies in the volume is the same in each sample. Picking the 700 largest galaxies excludes all galaxies less massive than about $8 \times 10^{10} h^{-1}{\rm M}_\odot$ or 30 gas particles. Picking the 300 largest galaxies corresponds to a minimum mass of approximately $1.5 \times 10^{11} h^{-1}{\rm M}_\odot$ or around 60 gas particles.

The correlation function has been calculated on scales of up to $25 h^{-1}$Mpc. This is half of the size of the simulation box, so the results presented here should not be treated as predictions of the true galaxy correlation function. Instead, the plots in Fig. 13 are intended to compare the relative clustering of GALFORM and SPH galaxies in our *small* simulation volume. All three models show qualitatively similar behaviour. When we consider the larger sample of galaxies (left panel in Fig. 13), we see an anti-bias relative to the dark matter on scales of less than a few h^{-1}Mpc, with galaxies tracing the dark matter on larger scales. This behaviour agrees with previous semi-analytic (e.g. Kauffmann et al. 1999; Benson et al. 2000) and SPH simulation (e.g. Pearce et al. 2001) results. If we include only the 300 most massive galaxies in the simulation volume (right panel in Fig. 13), we see that on large scales these more massive galaxies are more strongly clustered than the dark matter in all three cases.

The N-body GALFORM model with $f_{\rm df} = 0.5$ is in close agreement with the SPH simulation on scales larger than a few h^{-1}Mpc when we use the 700 most massive galaxies. This is to be expected since we have the same distribution of dark matter halos in each case and the merger rate in the semi-analytic model has been adjusted to reproduce roughly the distribution of galaxy masses in the simulation. On length scales smaller than this, where the correlation function is sensitive to the details of our treatment of galaxy mergers within halos, there is a difference of almost a factor of 2 between the SPH simulation and the GALFORM model with $f_{\rm df} = 0.5$. The treatment of mergers in this model reproduces the overall distribution of galaxy masses but the merger rates and galaxy distributions in halos of a given mass may not be in close agreement. When we merge GALFORM galaxies by associating them with groups of cold gas in the SPH simulation (short dashed lines in Fig. 13), the correlation functions agree to within about 25% on these small scales. If we consider only the 300 most massive galaxies in each case, the correlation function for the model with $f_{\rm df} = 0.5$ drops to almost an order of magnitude below that

of the SPH simulation on scales of about $0.3h^{-1}$Mpc. Again, this is due to differences in the merger rates in halos of a given mass since the discrepancy disappears if we use our SPH-based merging algorithm.

5 CONCLUSIONS

In this paper we have developed a method for calculating halo merger histories from N-body simulations and incorporated these merger histories into the GALFORM semi-analytic model of Cole et al. (2000). We carried out a comparison between this new "N-body GALFORM" model and the standard GALFORM model (which used Monte-Carlo merger trees) and identified reasons for the differences between the two models — most importantly the limited mass resolution imposed by the simulation on the merger trees and the slightly different distribution of progenitor masses for halos of a given mass. Once these differences have been accounted for, the two models are in very good agreement.

We produced a version of the N-body GALFORM model in which we ignored the effects of star formation and feedback, which we used to model an SPH simulation which also neglected these phenomena. In order to mimic the effect of the SPH smoothing kernel on the cooling rate in low mass halos we artificially increased the cooling time for gas in small halos in the semi-analytic model.

We compared properties of halos in the simulation with the properties of the same halos in the N-body GALFORM model. First, we looked at a global property of the halo population, the average fraction of cooled gas at redshift $z = 0$ as a function of halo mass. We found that a gas density profile with an initially small core radius which is able to increase with time was required to match the mean cold gas fractions seen in the SPH simulation. The level of agreement was excellent for halos with masses above the resolution limit of the SPH simulation.

Our method also enabled us to examine individual halos in the two cases. For the two gas density profiles described above, the total mass of cold gas in each halo was found to be in remarkably good agreement at cold gas masses greater than about $10^{12}h^{-1}\mathrm{M}_{\odot}$. In poorly resolved halos with lower cold gas masses the scatter in this relation increased substantially, to a factor of about 3. We found that much of the cold gas found in the more massive halos in the N-body GALFORM model generally cooled at later times than the gas in the same halos in the SPH simulation. By a redshift of 2 in the N-body GALFORM case, the progenitors of the halos contained only half as much cold gas as was present in the simulation. As the redshift increases, the mass of cold gas in the SPH simulation becomes dominated by material which cooled in very small halos, where the cooling rate may be strongly affected by resolution effects and depends sensitively on the SPH implementation (Springel et al. 2002). We are unable to model the SPH simulation in this regime, and so the GALFORM and SPH cold gas masses diverge as we go to higher redshifts.

We then turned our attention to the properties of individual galaxies at redshift $z = 0$. Our best fit model gave a distribution of galaxy masses in reasonable agreement with those in the SPH simulation for galaxies of more than 32 particles when we used the merger time scale of Cole et al. (2000), although the N-body GALFORM model contained a somewhat greater number of low mass galaxies and fewer very massive galaxies than were seen in the simulation. Doubling the merger rate in the GALFORM model improved the agreement at all masses, but note that the merger rates in the SPH simulation may not be reliable due to the effects of artificial viscosity (Frenk et al. 1996).

The dynamical friction treatment of merging used by our semi-analytic model precludes a direct comparison of individual galaxies. In order to circumvent this we suppressed all merging in the N-body GALFORM model and then used information from the SPH simulation to merge the resulting semi-analytic galaxies and to associate the merged galaxies with groups of cold gas particles in the simulation. This gave us a semi-analytic mass for each galaxy in the SPH simulation. We found that these masses were generally similar (within about 50% for larger galaxies) with a scatter close to that seen in the comparison of halo cold gas masses.

Finally, we examined the clustering properties of the more massive galaxies in the SPH simulation and two N-body GALFORM models. The first GALFORM model used the dynamical friction treatment of galaxy mergers, the second used our SPH merging scheme. We found that the correlation functions of galaxies in both GALFORM models agreed well with the SPH simulation on scales larger than typical group and cluster sizes, but that on scales of a few h^{-1}Mpc or less the correlation function of galaxies in the GALFORM model with dynamical friction induced merging was higher by almost a factor of 2. Using the SPH merging scheme reduced this discrepancy to about 25%, although some improvement was inevitable because this approach puts semi-analytic galaxies at the positions of groups of cold particles found in the SPH simulation.

In conclusion, our comparison shows that it is possible to closely model cooling, and to a lesser extent galaxy merger rates, in an SPH simulation using semi-analytic methods. Benson et al. demonstrated that the overall rate of cooling, globally and in halos of a given mass, predicted by SPH and semi-analytic models show remarkable consistency. Here we have shown that, with only minor changes to the semi-analytic model, very close agreement can be obtained on a halo by halo basis when merger trees are taken from the SPH simulation. Given the quite different limitations and assumptions inherent in the two techniques, this is a remarkable result. While we have allowed ourselves freedom to adjust the semi-analytic model in order to maximise the level of agreement with the simulation, it should be noted that in our best fit model, the only changes we have made to the cooling model of Cole et al. are a smaller core in the gas density profile and an increased cooling time in small halos. Neither of these changes have a large effect on the mean cold gas fraction at $z = 0$.

As well as providing evidence to support the treatment of cooling in current semi-analytic galaxy formation models, these results show that semi-analytic modelling provides a convenient, alternative way to add a baryonic component to an N-body simulation, which is at least as reliable as an SPH simulation. When used to investigate star formation and feedback prescriptions this approach allows the investigation of large regions of parameter space at little compuational cost and so can provide an indication of how these

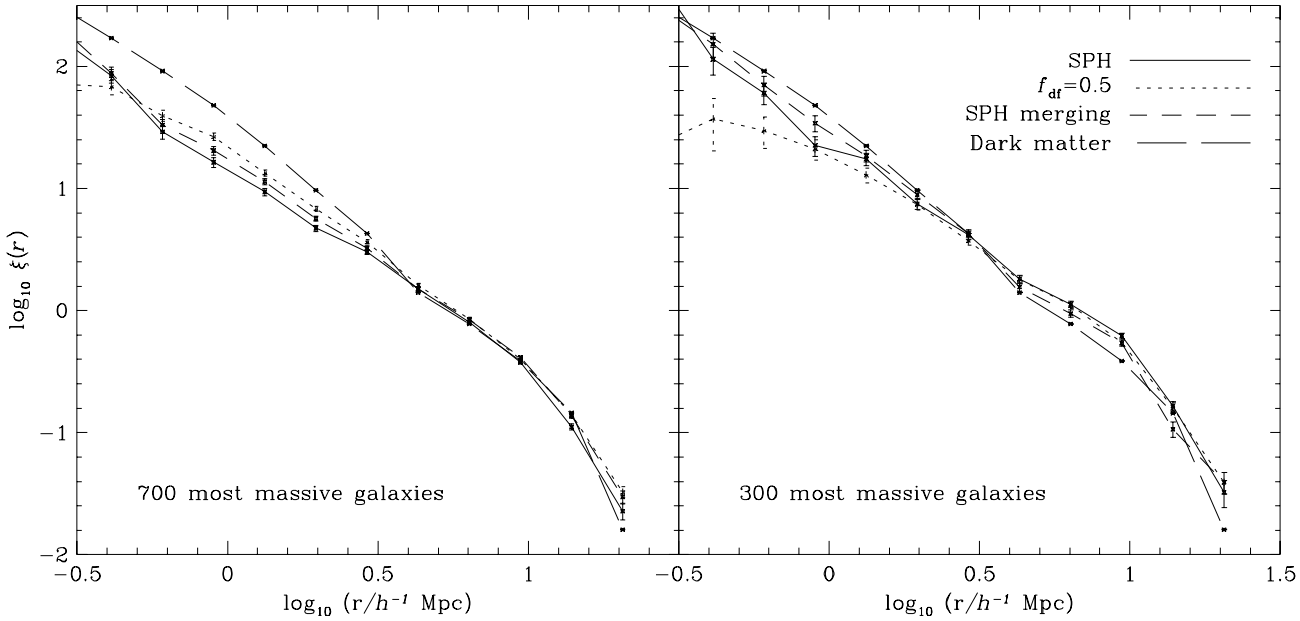

Figure 13. Two point galaxy correlation functions for three different models - the SPH simulation (solid lines), an N-body GALFORM model with merger rate parameter $f_{\rm df} = 0.5$ (dotted lines) and an N-body GALFORM model using the SPH based merger scheme described in Section 4.1.2 (short dashed lines). The long dashed lines show the correlation function for the dark matter in the SPH simulation. The 700 most massive galaxies in each case are included in the calculation for the left panel and only the 300 most massive galaxies are included in the right panel. Both N-body GALFORM models have a gas density profile with a core radius which is allowed to grow from an initial value of $r^0_{\rm core} = 0.15 r_{\rm NFW}$.

phenomena may be included in full hydrodynamic simulations.

Acknowledgements

We acknowledge support from PPARC and the Royal Society.

REFERENCES

Benson, A. J., Cole, S., Frenk, C. S., Baugh, C. M., Lacey, C. G., 2000, MNRAS, 311, 793
Benson, A.J., Pearce, F.R., Frenk, C.S., Baugh, C.M., Jenkins, A., 2001, MNRAS, 320, 261
Benson, A.J., Frenk, C.S., Baugh, C.M., Cole, S., Lacey, C.G., 2001, MNRAS, 327, 1041
Bond, J.R., Efstathiou, G., Kaiser, N., 1991, ApJ, 379, 440
Bower, R.G., 1991, MNRAS, 248, 332
Cen, R., Ostriker, J.P., 2000, ApJ, 538, 83
Cole, S., 1991, ApJ, 367, 45
Cole, S., Aragon-Salamanca, A., Frenk, C.S., Navarro, J.F., Zepf, S.E., 1994, MNRAS, 271, 781
Cole, S., Lacey, C.G., 1996, MNRAS, 281, 716
Cole S., Lacey C.G., Baugh C.M., Frenk C.S., 2000, MNRAS, 319, 168
Couchman, H.M.P., Thomas, P.A., Pearce, F.R., 1995, ApJ, 452, 797
Davis, M., Efstathiou, G., Frenk C.S., White, S.D.M, 1985, ApJ, 292, 371
Evrard, A.E., Summers, F.J., Davis, M., 1994, ApJ, 422, 11
Frenk, C.S., Evrard, A.E., White, S.D.M., Summers, F.J., 1996, ApJ, 472, 460
Gingold, R.A., Monaghan, J.J., 1977, MNRAS, 181, 375
Governato, F., Babul, A., Quinn, T., Tozzi, P., Baugh, C. M., Katz, N., Lake, G., 1999, MNRAS, 307, 949
Gross, M.A.K., Somerville, R.S., Primack, J.R., Holtzman, J., Klypin, A., 1998, MNRAS, 301, 81
Jenkins, A., Frenk, C.S., White, S.D.M., Colberg, J.M., Cole, S., Evrard, A.E., Couchman, H.M.P., Yoshida, N., 2001, MNRAS, 321, 372
Jenkins, A., Frenk, C. S., Pearce, F. R., Thomas, P. A., Colberg, J. M., White, S. D. M., Couchman, H. M. P., Peacock, J. A., Efstathiou, G., Nelson, A. H., 1998, ApJ, 499, 20
van Kampen, E., Jimenez, J., Peacock, J.A., 1999, MNRAS, 310, 43
Katz, N., Hernquist, L., Weinberg, D.H., 1992, ApJ, 399, L109
Katz, N., Weinberg, D.H., Hernquist, L., 1996, ApJS, 105, 19
Kauffmann, G., Colberg, J.M., Diaferio, A., White, S.D.M., 1999, MNRAS, 303, 188
Kauffmann, G., White, S.D.M., 1993, MNRAS, 261,921
Lacey, C.G., Cole, S., 1994, MNRAS, 271, 676
Lacey, C.G., Cole, S., 1993, MNRAS, 262, 627
Lacey, C.G., Silk, J., 1991, ApJ, 381, 14
Lucy, L.B., 1977, AJ, 82, 1013
Navarro, J.F., Frenk, C.S., White, S.D.M., 1995, MNRAS, 275, 720
Navarro, J.F., Frenk, C.S., White, S.D.M., 1996, ApJ, 462, 563
Navarro, J.F., Frenk, C.S., White, S.D.M., 1997, ApJ, 490, 493
Navarro, J.F., Steinmetz, M., 1999, ApJ, 513, 555
Navarro, J.F., White, S.D.M., 1993, MNRAS, 265, 271
Pearce, F.R., Couchman, H.M.P., 1997, New Astronomy, 2 ,411
Pearce, F.R., Jenkins, A., Frenk, C.S., White,S.D.M., Thomas, P.A., Couchman, H.M.P., Peacock, J.A., Efstathiou, G., 2001, MNRAS, 326, 649

Pearce, F.R., Jenkins, A., Frenk, C.S., Colberg, J.M., White, S.D.M., Thomas, P.A., Couchman, H.M.P., Peacock, J.A., Efstathiou, G. (The VIRGO Consortium), 1999, ApJ, 521, 99
Press, W.H., Schechter, P., 1974, ApJ, 187, 425
Roukema, B.F., Peterson, B.A., Quinn, P.J., Rocca-Volmerange, B., 1997, MNRAS, 292, 835
Somerville, R.S., Primack, J.R., 1999, MNRAS, 310, 1087
Springel, V., Hernquist, L., MNRAS, in press, astro-ph/0111016
Springel, V., White, S.D.M., Tormen, G., Kauffmann, G., 2001, MNRAS, 328, 726
Steinmetz, M., Müller, E., 1995, MNRAS, 276, 549
Sutherland, R., Dopita, M., 1993, ApJS, 88, 253
Tormen, G., 1997, MNRAS, 300, 773
Tormen, G., 1998, MNRAS, 297, 648
Wechsler, Risa H., Somerville, Rachel S., Bullock, James S., Kolatt, Tsafrir S., Primack, Joel R., Blumenthal, George R., Dekel, Avishai, 2001, ApJ, 554, 85
White, S.D.M., Frenk, C.S., 1991, ApJ, 379, 52
White, S.D.M., Rees, M.J., 1978, MNRAS, 183, 341